Behavioral/Cognitive

Threat and Bidirectional Valence Signaling in the Nucleus Accumbens Core

Madelyn H. Ray*, Mahsa Moaddab*, and Michael A. McDannald
Department of Psychology and Neuroscience, Boston College, Chestnut Hill, Massachusetts 02467

Appropriate responding to threat and reward is essential to survival. The nucleus accumbens core (NAcc) is known to support and organize reward behavior. The NAcc is also necessary to fully discriminate threat and safety cues. To directly reveal NAcc threat firing, we recorded single-unit activity from seven female rats undergoing pavlovian fear discrimination. Rats fully discriminated danger, uncertainty, and safety cues, and most NAcc neurons showed the greatest firing change to danger and uncertainty. Heterogeneity in cue and reward firing led us to identify distinct functional populations. One NAcc population signaled threat, specifically decreasing firing to danger and uncertainty cues. A separate population signaled Bidirectional Valence, decreasing firing to the danger cue (negative valence), but increasing firing to reward (positive valence). The results reveal the NAcc to be a source of threat information and a more general valence hub.

Key words: **associative learning; fear; single unit; ventral striatum**

Significance Statement

The nucleus accumbens core (NAcc) is synonymous with reward. Yet, anatomy, neurotoxic lesions, and optogenetic manipulation implicate the NAcc in threat. Here, we directly revealed NAcc threat firing by recording single-unit activity during multicue fear discrimination. Most cue-responsive NAcc neurons markedly altered firing to threat cues. Finer analyses revealed a NAcc population signaling threat, specifically decreasing firing to danger and uncertainty cues; and a NAcc population signaling Bidirectional Valence, increasing firing to reward but decreasing firing to the danger cue. The results reveal the NAcc to be a source of threat information and a valence hub.

Introduction

Appropriate responding to reward and threat is essential to survival. Rather than leave encounters with positive and negative valence events to chance, animals form predictions about their occurrence. The nucleus accumbens plays a well established role in learning about and organizing behaviors toward positive valence outcomes and their predictive cues, particularly for food rewards (Baldo and Kelley, 2007; Carlezon and Thomas, 2009; Basar et al., 2010; Mannella et al., 2013; Klawonn and Malenka, 2018). The nucleus accumbens is primarily composed of two functionally and anatomically distinct subregions: the core and the shell (Voorn et al., 1989; Zahm and Brog, 1992). The nucleus accumbens core (NAcc) is central to reward-related behavior. NAcc lesions or pharmacological manipulations decrease responding to reward-predictive cues (Parkinson et al., 1999a, 2000; Di Ciano et al., 2008; Floresco et al., 2008; Blaiss and Janak, 2009; Chaudhri et al., 2010; Ambroggi et al., 2011; Corbit and Balleine, 2011; Fraser and Janak, 2017). NAcc neurons encode various aspects of reward (Roesch et al., 2009; Krause et al., 2010; McGinty et al., 2013; Sugam et al., 2014; Sicre et al., 2020). For example, NAcc neurons show greater firing increases in response to a reward-predictive cue compared with a neutral cue (Cerri et al., 2014) and preferentially respond to a discriminative stimulus that signals reward availability via firing excitations and inhibitions (Nicola et al., 2004; Ambroggi et al., 2011). In addition to signaling palatability (Roitman et al., 2005; Taha and Fields, 2005), NAcc neurons track relative reward value across a variety of conditions, showing firing increases to outcome presentation that scale to the value of a reward (Ottenheimer et al., 2018).

The NAcc is also necessary for learning and behavior pertaining to negative valence. Discrimination procedures using sucrose and quinine outcomes have found that a substantial portion of nucleus accumbens neurons acquire firing to quinine and its predictive cue (Setlow et al., 2003; Roitman et al., 2005). Accumbens lesions centered on the core disrupt the increased latencies of "go" responses to quinine cues (Schoenbaum and Setlow, 2003). Further, brief optogenetic simulation of the accumbens can induce approach, while prolonged stimulation

Received May 26, 2021; revised Oct. 29, 2021; accepted Nov. 4, 2021.

Author contributions: M.H.R. and M.A.M. designed research; M.H.R. and M.A.M. performed research; M.H.R., M.M., and M.A.M. analyzed data; M.M. and M.A.M. wrote the paper.

This research was supported by National Institutes of Health/National Institute of Mental Health Grant R01-MH-117791. The content is solely the responsibility of the authors and does not necessarily represent the official views of the National Institutes of Health. We thank Bret Judson and the Boston College Imaging Core for infrastructure/support, and Dr. Maureen Ritchey for discussions on firing similarity analyses.

*M.H.R. and M.M. contributed equally to this work.

The authors declare no competing financial interests.

Correspondence should be addressed to Michael A. McDannald at michael.mcdannald@bc.edu.

https://doi.org/10.1523/JNEUROSCI.1107-21.2021

can induce avoidance (Soares-Cunha et al., 2020). Negative valence tastes, such as quinine, and their predictive cues produce a highly specific suite of behavioral and orofacial responses (Grill and Norgren, 1978; Kerfoot et al., 2007; Berridge, 2019). Whereas footshock-associated cues produce a distinct suite of defensive behaviors: freezing, hyperventilation, piloerection, suppression of reward-related behavior, and more (Estes and Skinner, 1941; Bolles, 1970; Bolles and Collier, 1976; Bouton and Bolles, 1980). It is unclear how individual NAcc neurons respond to cues under the threat domain of negative valence.

The NAcc has not been viewed as a major node in the threat network of brain. This title is often bestowed on the amygdala (LeDoux et al., 1990; Campeau and Davis, 1995; Killcross et al., 1997; Koo et al., 2004). While the amygdala is undoubtedly important, threat learning and behavior is normally the product of a much larger network (Beck and Fibiger, 1995; Vetere et al., 2017; Morrow et al., 2021). This network includes traditional "reward" regions (Reynolds and Berridge, 2002; Pauli et al., 2015; Bouchet et al., 2018; Groessl et al., 2018; Cai et al., 2020; Piantadosi et al., 2020; Stephenson-Jones et al., 2020; Moaddab et al., 2021; Moaddab and McDannald, 2021). The NAcc receives a prominent, direct projection from the basolateral amygdala (Christie et al., 1987; Kita and Kitai, 1990; Brog et al., 1993). Footshock-associated cues and contexts increase NAcc immediate early gene expression (Beck and Fibiger, 1995; Thomas et al., 2002). Indeed, there is a growing body of evidence implicating the NAcc in a variety of threat processes (Iordanova et al., 2006; Martinez et al., 2008; Badrinarayan et al., 2012; Budygin et al., 2012; Wenzel et al., 2015; Zhang et al., 2020). However, studies aimed at determining the role of NAcc in fear using traditional cued and contextual conditioning procedures have produced conflicting results (Parkinson et al., 1999b; Levita et al., 2002; Schwienbacher et al., 2004; Wendler et al., 2014).

The NAcc is necessary to scale fear to degree of threat (Ray et al., 2020). Using a conditioned suppression procedure consisting of cues predicting unique footshock probabilities [danger ($p = 1.00$), uncertainty ($p = 0.25$), and safety ($p = 0.00$)], we have shown that the NAcc is necessary to acquire complete fear discrimination. We further uncovered a specific role for the NAcc in the acquisition and expression of rapid uncertainty–safety discrimination. Here, we set out to reveal NAcc threat firing. We recorded single-unit activity from female rats undergoing fear discrimination. First, we sought to reveal whether NAcc neurons are responsive to threat cues. If so, we could then determine the specificity and diversity of NAcc threat firing. Last, using suppression of rewarded nose poking as our fear measure allowed us to compare threat and reward-related firing. Our behavior/recording approach allowed us to uncover signals specific to threat, as well as signals for Bidirectional Valence (Stephenson-Jones et al., 2020; Vento and Jhou, 2020; Moaddab et al., 2021).

Materials and Methods

The recording/fear discrimination approach is based on prior work from our laboratory (Moaddab et al., 2021).

Subjects

Seven female Long–Evans rats were bred in the Boston College Animal Care Facility. Behavioral testing took place in adulthood when rats weighed 215–300 g. Rats were single housed on a 12 h light/dark cycle (lights on at 6:00 A.M.) with free access to water. Rats were maintained at 85% of their free-feeding body weight with standard laboratory chow (18% Protein Rodent Diet #2018, Harlan Teklad Global Diets), except during surgery and postsurgery recovery. All protocols were approved by the Boston College Animal Care and Use Committee, and all experiments were conducted in accordance with the National Institutes of Health guidelines regarding the care and use of rats for experimental procedures.

Electrode assembly

Microelectrodes consisted of a drivable bundle of 16 25.4-μm-diameter Formvar-Insulated Nichrome Wire (catalog #761500, A-M Systems) within a 27 gauge cannula (catalog #B000FN3M7K, Amazon Supply) and two 127-μm-diameter paraformaldehyde (PFA)-coated, annealed strength stainless steel ground wires (catalog #791400, A-M Systems). All wires were electrically connected to a Nano Strip (catalog #A79042-001, Omnetics Connector Corporation) on a custom 24-contact, individually routed, and gold-immersed circuit board (San Francisco Circuits). The 16-wire bundle was integrated into a microdrive permitting advancement in ~42 μm increments.

Surgery

Aseptic, stereotaxic surgery was performed under isoflurane anesthesia (1–5% in oxygen). Carprofen (5 mg/kg, s.c.) and lactated Ringer's solution (10 ml, s.c.) were administered preoperatively. The skull was scoured in a crosshatch pattern with a scalpel blade to increase surface area. Six screws were installed in the skull. A 1.4-mm-diameter craniotomy was performed to remove a circular skull section centered on the implant site, and the underlying dura was removed to expose the cortex. Nichrome recording wires were freshly cut with surgical scissors to extend ~2.0 mm beyond the cannula. Just before implant, current was delivered to each recording wire in a saline bath, stripping each tip of its formvar insulation. Current was supplied by a 12 V lantern battery, and each Omnetics connector contact was stimulated for 2 s using a lead. Machine grease was placed around the cannula and microdrive. For implantation dorsal to the NAcc, the electrode assembly was slowly advanced (~100 μm/min) to the following coordinates relative to bregma: +1.44 mm anterior, −1.40 mm lateral, and −6.00 mm ventral from the cortex. Once in place, stripped ends of ground wires were wrapped around two screws, and screws were advanced to contact cortex. The microdrive base and a protective head cap were cemented in place with orthodontic resin (catalog #C 22–05-98, Pearson Dental Supply), and the Omnetics connector was affixed to the head cap.

Behavioral apparatus

All experiments were conducted in two behavioral chambers housed in sound-attenuating shells. Behavioral chambers had aluminum front and back walls retrofitted with clear plastic covers, clear acrylic sides and top, and a stainless steel grid floor. Each grid floor bar was electrically connected to an aversive shock generator (Med Associates) through a grounding device. The grounding device permitted the floor to be always grounded except during shock delivery. An external food cup and a central port, equipped with infrared photocells, were present on one wall. Auditory stimuli were presented through two speakers mounted on the ceiling of enclosure. Behavior chambers were modified to allow for free movement of the electrophysiology cable during behavior, plastic funnels were epoxied to the top of the behavior chambers with the larger end facing down, and the tops of the chambers were cut to the opening of the funnel.

Nose poke acquisition

Rats were pre-exposed to the experimental pellets in their home cages (Bio-Serv). Rats were then shaped to nose poke for pellet delivery in the behavior chamber using a fixed ratio schedule in which one nose poke yielded one pellet. Over the next 5 days, rats were placed on variable interval (VI) schedules in which nose pokes were reinforced on average every 30 s (VI-30, day 1) and 60 s (VI-60, days 2 through 5). Nose pokes were reinforced on a VI-60 schedule throughout fear discrimination independent of cue and shock presentation. We use the VI-60 reinforcement schedule, rather than a fixed ratio schedule, to promote consistent nose poking across the session and between individuals. Stable nose

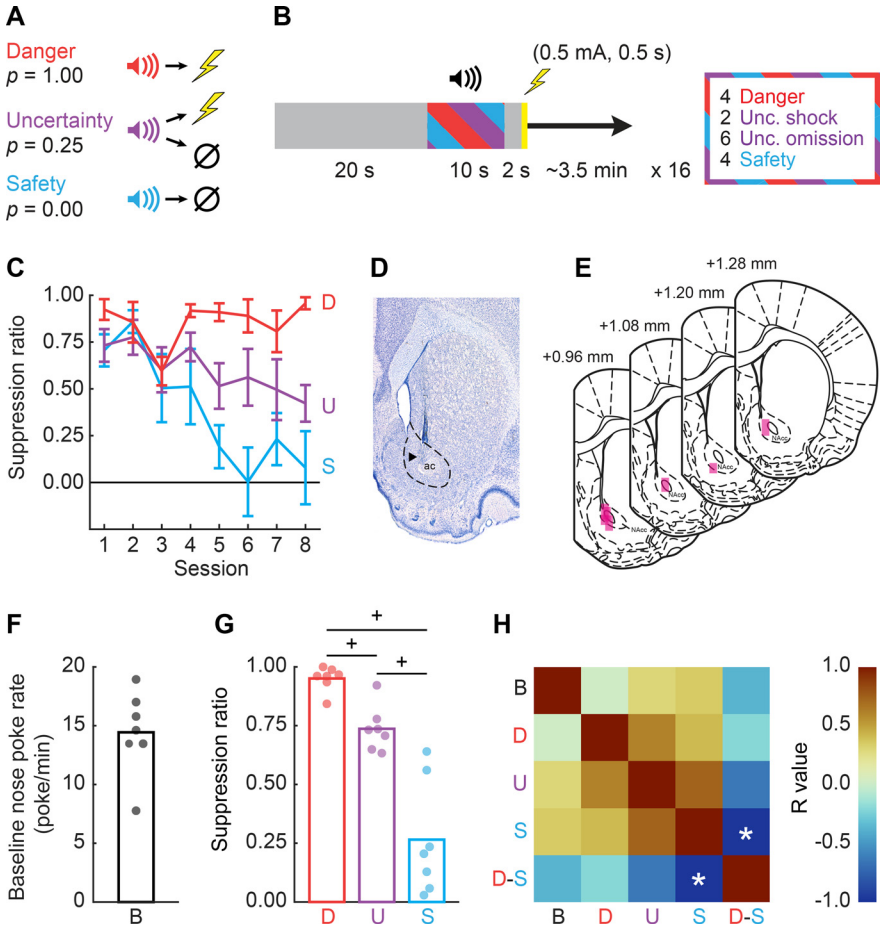

Figure 1. Fear discrimination, histology, and behavior. ***A***, Pavlovian fear discrimination consisted of three auditory cues, each associated with a unique probability of footshock: danger ($p = 1.00$, red), uncertainty ($p = 0.25$, purple), and safety ($p = 0.00$, blue). ***B***, Each trial started with a 20 s baseline period followed by 10 s cue period. Footshock (0.5 mA, 0.5 s) was administered 2 s following the cue offset in shock and uncertainty shock trials. Each session consisted of 16 trials: 4 danger trials, 2 uncertainty shock trials, 6 uncertainty omission trials, and 4 safety trials with an average intertrial interval (ITI) of 3.5 min. ***C***, Mean ± SEM suppression ratios to danger (D; red), uncertainty (U; purple), and safety (S; blue) cues are shown for the initial eight fear discrimination sessions. ***D***, Example of a Nissl-stained NAcc (outlined in black) section showing the location of the recording site within the boundaries of the NAcc. ***E***, Histologic reconstruction of microelectrode bundle placements ($n = 7$) in the NAcc are represented by pink bars, bregma levels indicated. ***F***, Mean (bar) and individual (data points, $n = 7$) baseline nose poke rate (B; black) is shown for each rat. ***G***, Mean (bar) and individual subject (data points, $n = 7$) suppression ratio for each cue (D, red; U, purple; S, blue) is shown. $^{+}$95% bootstrap confidence interval for differential suppression ratio does not contain zero. ***H***, Correlation matrices among individual baseline nose poke rate (B), cue suppression ratio (D, red; U, purple; S, blue), and overall discrimination (danger suppression ratio − safety suppression ratio) are depicted. Color scale for correlation coefficient (R) is shown to the right, with perfect positive correlation dark red ($R = 1$) and perfect negative correlation dark blue ($R = -1$). *Pearson's correlation, $p < 0.05$. Mean individual suppression ratios are shown in Extended Data Figure 1-1, and session × session individual suppression ratios are shown in Extended Data Figure 1-2.

poking allows a precise measure of fear with conditioned suppression (Kamin et al., 1963; McAllister, 1997; Piantadosi et al., 2020).

Experimental design and statistical analysis

Before surgery, each rat received eight 54 min pavlovian fear discrimination sessions. Each session consisted of 16 trials, with a mean intertrial interval of 3.5 min. Auditory cues were 10 s repeating motifs of patterned beep, broadband click, phaser, or trumpet (listen or download: http://mcdannaldlab.org/resources/ardbark). Each cue was associated with a unique footshock probability (0.5 mA, 0.5 s), as follows: danger, $p = 1.00$; uncertainty, $p = 0.25$; and safety, $p = 0.00$. Auditory identity was counterbalanced across rats. For danger and uncertainty shock trials, footshock was administered 2 s following cue offset. A single session consisted of four danger trials, two uncertainty shock trials, six uncertainty omission trials, and four safety trials, with order randomly determined by the behavioral program (Fig. 1*A*,*B*). After the eighth discrimination session, rats were given *ad libitum* food access and implanted with drivable microelectrode bundles. Following surgical recovery, discrimination resumed with single-unit recording. The microelectrode bundles were advanced in steps of ~42–84 μm every other day to record from new single units during the following session.

Single-unit data acquisition. During recording sessions, a 1× amplifying head stage connected the Omnetics connector to the commutator via a shielded recording cable (head stage: catalog #40684–020; cable: catalog #91809–017, Plexon). Analog neural activity was digitized and high-pass filtered via amplifier to remove low-frequency artifacts and then were sent to the OmniPlex D Acquisition System (Plexon). Behavioral events (cues, shocks, nose pokes, and rewards) were controlled and recorded by a computer running Med Associates software. Time-stamped events from Med Associates were sent to the OmniPlex D Acquisition System via a dedicated interface module (catalog #DIG-716B, Med Associates). The result was a single file (.pl2) containing all time stamps for recording and behavior. Single units were sorted offline using principal components analysis and a template-based spike-sorting algorithm (Offline Sorter V3, Plexon). Time-stamped spikes and events (cues, shocks, nose pokes, rewards) were extracted and analyzed with statistical routines in MATLAB.

Histology. Rats were deeply anesthetized using isoflurane, and final electrode coordinates were marked by passing current from a 6 V battery through 4 of the 16 nichrome wires. Rats were transcardially perfused with 0.9% biological saline and 4% paraformaldehyde in a 0.2 M potassium phosphate-buffered solution. Brains were extracted and postfixed in a 10% neutral-buffered formalin solution for 24 h, stored in 10% sucrose/formalin, frozen at −80°C, and sectioned via microtome. Nissl staining was performed to identify NAcc boundaries. Sections were mounted on coated glass slides, Nissl stained, coverslipped with OmniMount Mounting Medium (Thermo Fisher Scientific), and imaged using a light microscope (model Axio Imager Z2, Zeiss).

Verifying electrode placement. Passing current through the wire permitted tip locations to be identified in brain sections. In addition, wire tracks leading up to tips were visible. Starting with the electrode tips, the driving path of the electrode through the brain was calculated backward. Only single units obtained from recording locations inside of the tear-shaped region surrounding the anterior commissure (Paxinos and Watson, 2007) were considered to be in the NAcc (Fig. 1*D*,*E*), and therefore only these single units were included in analyses.

Bootstrap confidence intervals. The 95% bootstrap confidence intervals (CIs) were constructed for suppression ratios, normalized firing rates, and beta coefficients using the bootci function in MATLAB. Bootstrap distributions were created by sampling the data 1000 times with replacement. Studentized confidence intervals were constructed, with the critical outputs being the mean, lower bound, and upper bound of the 95% bootstrap confidence interval. The 95% bootstrap confidence intervals were used to compare suppression ratios and normalized firing

rates between cues, as well as to zero. The 95% bootstrap confidence intervals were also used to compare beta coefficients between regressors and to zero. Null-hypotheses stating that no differences were observed in any case were supported when zero fell within the upper and lower bounds of the of the 95% bootstrap confidence interval. Differences were said to be observed when the 95% bootstrap confidence interval did not contain zero.

Calculating suppression ratios. Fear was measured by suppression of rewarded nose poking, calculated as the following ratio: [(baseline nose poke rate – cue nose poke rate)/(baseline nose poke rate + cue nose poke rate)]. The baseline nose poke rate was taken from the 20 s before cue onset (Fig. 1*F*), and the cue poke rate from the 10 s cue period. Suppression ratios were calculated for each trial using only the baseline of that trial. A ratio of 1 indicated high fear, 0 indicated low fear, and gradations between them indicated intermediate levels of fear. Suppression ratios were analyzed using ANOVA with cue (danger, uncertainty, safety) and session (1–8; Fig. 1*C*) or cue (Fig. 1*G*) as a factor. *F* statistic, *p* value, partial eta squared (η_p^2), and observed power (op) are reported for significant main effects and interactions. Mean individual baseline nose poke rates and suppression ratios were visualized using the plotSpread function in MATLAB (https://www.mathworks.com/matlabcentral/fileexchange/37105-plot-spread-points-beeswarm-plot).

Behavior correlation matrix. Relationships among individual baseline nose poke rate, cue suppression ratio (danger, uncertainty, safety), and overall discrimination (danger suppression ratio – safety suppression ratio) were determined by calculating the *R* and *p* values for Pearson's correlation coefficient (Fig. 1*H*).

Identifying cue-responsive neurons. Single units were screened for cue responsiveness by comparing mean firing rate (in hertz) during the 10 s baseline period just before cue onset, to mean firing rate (in hertz) during the first 1 s and the last 5 s of danger, uncertainty, and safety using a paired, two-tailed *t* test ($p < 0.05$). The 1 s and the last 5 s of cue presentation were selected because these time windows best captured NAcc firing patterns. A single unit was considered to be cue responsive if it showed a significant increase or decrease in firing from baseline to danger, uncertainty, or safety during the first 1 s or the last 5 s interval. Bonferroni correction was not performed because this criterion was too stringent, resulting in obviously cue-responsive neurons being omitted from analysis.

Firing and waveform characteristics. The following characteristics were determined for our three main populations: baseline firing rate (in hertz), coefficient of variance, and waveform peak–valley duration (see Fig. 3). Baseline firing rate was the mean firing rate (in hertz) during the 10 s period just before cue onset. Coefficient of variance was calculated by $[SD_{ISI}/\overline{X}_{ISI}]$, in which SD_{ISI} was the SD of interspike interval, and $\overline{X}_{ISI}$ was the mean interspike interval. Coefficient of variance is a relative measure of the variability of spike firing, with small values indicating less variation in interspike intervals (more regular firing), and large values indicating more variability (less regular firing; Saeb-Parsy and Dyball, 2003; Moaddab et al., 2015). Waveform peak–valley duration was the *x*-axis distance between the valley of depolarization and the peak of after-hyperpolarization, with smaller values indicating narrow waveforms (Gage et al., 2010; Gittis et al., 2011; Vachez et al., 2021).

K-means clustering. Clustering was performed using the MATLAB kmeans function. The firing rate of all cue-responsive neurons ($n = 193$) was summarized in a 193-neuron × 6-epoch matrix. The six firing epochs were mean onset (first 1 s) and late cue (last 5 s) firing for danger, uncertainty, and safety—the same periods used for selecting cue-responsive units. Clustering was performed seven times, incrementing from one to seven clusters. The primary result of clustering was the cluster membership of each neuron and the mean of the squared Euclidean distance between each cluster member and the cluster centroid. Cluster number was optimized to produce the fewest number of clusters and the smallest mean Euclidean distance of each cluster member from its centroid.

z-score normalization. For each neuron, and for each trial type, firing rate (in hertz) was calculated in 250 ms bins from 20 s before cue onset to 20 s following cue offset, for a total of 200 bins. Mean firing rate over the 200 bins was calculated by averaging all trials for each trial type. Mean differential firing was calculated for each of the 200 bins by subtracting mean baseline firing rate (10 s before cue onset), specific to that trial type, from each bin. Mean differential firing was *z*-score normalized across all trial types within a single neuron, such that the mean firing = 0, and SD in firing = 1. The *z*-score normalization was applied to firing across the entirety of the recording epoch, as opposed to only the baseline period, in case neurons showed little/no baseline activity. As a result, periods of phasic, excitatory, and inhibitory firing contributed to normalized mean firing rate (0). For this reason, *z*-score normalized baseline activity can differ from zero. The *z*-score normalized firing rate was analyzed with ANOVA using cue and bin as factors. *F* and *p* values are reported, as well as η_p^2 and op. To avoid contamination by cue and shock deliveries, reward-related firing was extracted from intertrial intervals, when no cues or footshocks were presented. Although not explicitly cued through the speaker, each reward delivery was preceded by a brief sound caused by the advance of the pellet feeder. For reward-related firing (time locked to pellet feeder advance), normalized firing rate was calculated in 250 ms bins from 2 s before 2 s following advancement of pellet feeder, for a total of 16 bins. The mean differential firing rate was calculated for each of the 16 bins by subtracting pre-reward firing rate (mean of 1 s before reward delivery).

Nose poke cessation events were identified by selecting a single nose poke followed by at least 2 s with no further pokes. Nose poke cessation-related firing was extracted from the intertrial interval, a period when no cues or footshocks were presented. For nose poke cessation firing, the normalized firing rate was calculated in 250 ms bins from 2 s before to 2 s following the identified nose poke, for a total of 16 bins. Examining this period ensures a nose poke rate of 0 in the final 2 s. Mean differential firing was calculated for each of the 16 bins by subtracting the pre-nose poke cessation firing rate (mean of 1 s before nose poke cessation).

Heat plot and color maps. Heat plots were constructed from the normalized firing rate using the imagesc function in MATLAB (Fig. 2, Extended Data Fig. 2-1). Perceptually uniform color maps were used to prevent visual distortion of the data (Scientific Colour Maps, version 4.0.0; https://www.fabiocrameri.ch/colourmaps/).

Population and single-unit firing analyses. Cue firing was analyzed using ANOVA with cue (danger, uncertainty, safety) and bin (250 ms bins from 2 s before cue onset to cue offset) as factors (see Figs. 4, 5). Uncertainty trial types were collapsed because they did not differ. This was expected because during cue presentation rats did not know the current uncertainty trial type. *F* statistic, *p* value, η_p^2, and op values are reported for main effects and interactions. The 95% bootstrap confidence intervals were reconstructed for normalized firing rate to each cue (compared with 0), as well as for differential firing rate (danger vs uncertainty; uncertainty vs safety; danger and uncertainty vs safety; and danger vs uncertainty and safety) during cue onset (first 1 s cue interval) and late cue (last 5 s cue interval). The distribution of single-unit firing was visualized using the plotSpread function for MATLAB. Reward firing was analyzed using repeated-measures ANOVA with bin (250 ms bins, from 2 s before to 2 s following advancement of pellet feeder) as a factor (see Fig. 9*A–D*). The 95% bootstrap confidence intervals were reconstructed for normalized firing to reward during pre-reward delivery (250 ms before reward delivery) and post-reward delivery (first 250 ms following reward delivery; compared with zero), as well as for differential firing (pre-reward delivery vs post-reward delivery). Relationships between cue firing (danger, 10 s cue; safety, the first 1 s cue) and reward (see Fig. 9*E–G*), as well as cue firing (danger, 10 s cue; safety, the first 1 s cue; see Fig. 9*H–J*) were determined by calculating the R^2 and *p* values for Pearson's correlation coefficient. A similar analysis was performed for nose poke cessation firing (see Fig. 10).

Tuning curve. Single-unit, linear regression was used to determine the cue-firing pattern best describing each neuron (see Fig. 7). Five separate regression analyses were performed. For each, all 16 trials (4 danger, 8 uncertainty, and 4 safety) from a single session were ordered by type. For each single unit, the mean normalized firing rate for each 10 s cue was calculated. The cue pattern regressor assigned values to each trial type. The values for danger (1.00) and safety (0.00) were fixed. A tuning curve was constructed by systematically increasing the value assigned to uncertainty from 0 to 1 in 0.25 steps (0.00, 0.25, 0.50, 0.75, 1.00).

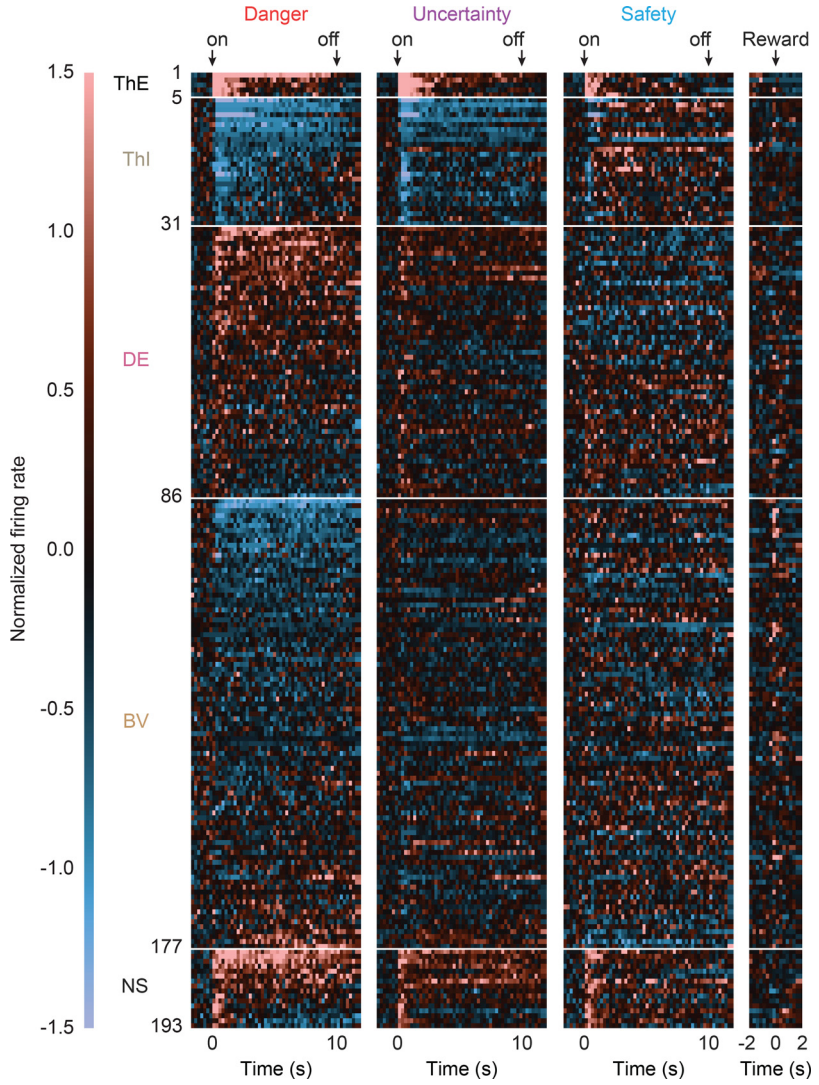

Figure 2. Heat plot of cue-responsive neurons. Mean normalized firing rate for each cue-responsive neuron ($n = 193$) for each of the three trial types (danger, uncertainty, and safety) in 250 ms bins (2 s before cue onset to 2 s following cue offset), as well as reward (2 s before to 2 s following reward delivery). Cue onset (on), offset (off), and reward are indicated by black arrows. All cue-responsive neurons are sorted by their responses to cues [ThE, Threat Excited ($n = 5$, black); ThI, Threat Inhibited ($n = 26$, gray); DE, Danger Excited ($n = 55$, pink); BV, Bidirectional Valence ($n = 91$, tan); NS, Non-Selective ($n = 16$, black)]. Color scale for normalized firing rate is shown to the left. A normalized firing rate of zero is indicated by the color black, with the greatest increases indicated by light red and the greatest decreases indicated by light blue. Alternative clustering heat plots are shown in Extended Data Figure 2-1.

Regression (using the regress function in MATLAB) required a separate, constant input. The regression output was the beta coefficient for each cue pattern regressor, quantifying the strength (greater distance from 0 = stronger) and direction (>0 = positive) of the predictive relationship between cue pattern regressor and single-unit firing at each uncertainty assignment level. The peak (for cue-excited single units) and trough (for cue-inhibited single units) of the tuning curve was the uncertainty assignment with the most extreme, mean beta coefficient value.

Single-unit linear regression. Linear regression was used to determine the degree to which single units signaled fear output and exaggerated threat before and across cue presentation. The *z*-score normalized firing rate was calculated in 1 s bins from 2 s before cue onset through cue presentation (12 total bins). The fear output regressor was the suppression ratio for the entire cue, for that specific trial. The cue pattern regressor used 1.00 for danger and 0.00 for safety and the uncertainty assignment reflecting the peak or trough of the tuning curve for that population. The regression output was the beta coefficient for each regressor (fear output, exaggerated threat), quantifying the strength (greater distance from 0 = stronger) and direction (>0 = positive) of the predictive relationship between each regressor and single-unit firing. ANOVA was used to analyze beta coefficients, with regressor (fear output, exaggerated threat) and bin (12, 1 s) as factors (see Fig. 8*A*,*C*,*E*).

Pitman–Morgan test. The Pitman–Morgan test is used to compare within-cluster variance in cue firing (safety vs danger, safety vs uncertainty; see Fig. 4*F*, left). The *p* values are reported for each test.

Hartigan's Dip Statistic. Hartigan's Dip Statistic is used to test whether the baseline firing rate (in hertz), coefficient of variance, and waveform peak–valley duration of each functional cluster had more than one mode in their distribution (Fig. 3). The *p* values are reported for each test, with $p < 0.05$ rejecting the null hypothesis that a distribution contained one mode, supporting the interpretation of a bimodal distribution.

Firing similarity analyses. For each neuron, mean normalized firing rates were calculated for danger, uncertainty, and safety (12, 1 s bins: 2 s before cue onset to cue offset). Firing similarity was quantified for each cue pair, for each neuron using Pearson's correlation coefficient. The result was an *R* value for each neuron–cue pair: danger versus uncertainty, uncertainty versus safety, and danger versus safety. ANOVA for *R* value was performed with cluster and comparison as factors. Within- and between-cluster *post hoc* comparisons were performed with Bonferroni *t* tests (see Fig. 6).

Data availability

The full electrophysiology dataset will be uploaded to http://crcns.org/ on acceptance for publication. Med Associates programs used for behavior and MATLAB programs used for behavioral analyses are freely available at our laboratory website: http://mcdannaldlab.org/resources.

Results

Female Long–Evans rats ($n = 7$) were moderately food deprived and trained to nose poke in a central port to receive a food reward. Nose poking was reinforced throughout fear discrimination, but poke–reward contingencies were independent of cue–shock contingencies. During fear discrimination (Fig. 1*A*,*B*), three auditory cues predicted unique footshock probabilities: danger ($p = 1.00$); uncertainty ($p = 0.25$); and safety ($p = 0.00$). Fear was measured with the suppression ratio, which was calculated by comparing nose poke rates during baseline and cue periods. A suppression ratio of 1 indicates complete nose poke suppression during cue presentation, 0 indicates no suppression, and values between 1 and 0 indicate gradations of suppression. Rats acquired discrimination over the first eight sessions, showing high suppression in response to danger, intermediate suppression in response to uncertainty, and low suppression in response to safety (Fig. 1*C*). ANOVA for suppression ratios [factors: cue (danger, uncertainty, safety) and session (1–8)] found a main effect of cue ($F_{(2,12)} = 24.49$, $p = 6.00 \times 10^{-5}$, $\eta_p^2 = 0.80$, op = 1.00), and a cue × session interaction ($F_{(14,84)} = 4.57$, $p = 5.00 \times 10^{-6}$, $\eta_p^2 = 0.43$, op = 1.00). Rats were next implanted with drivable, 16-wire microelectrode bundles

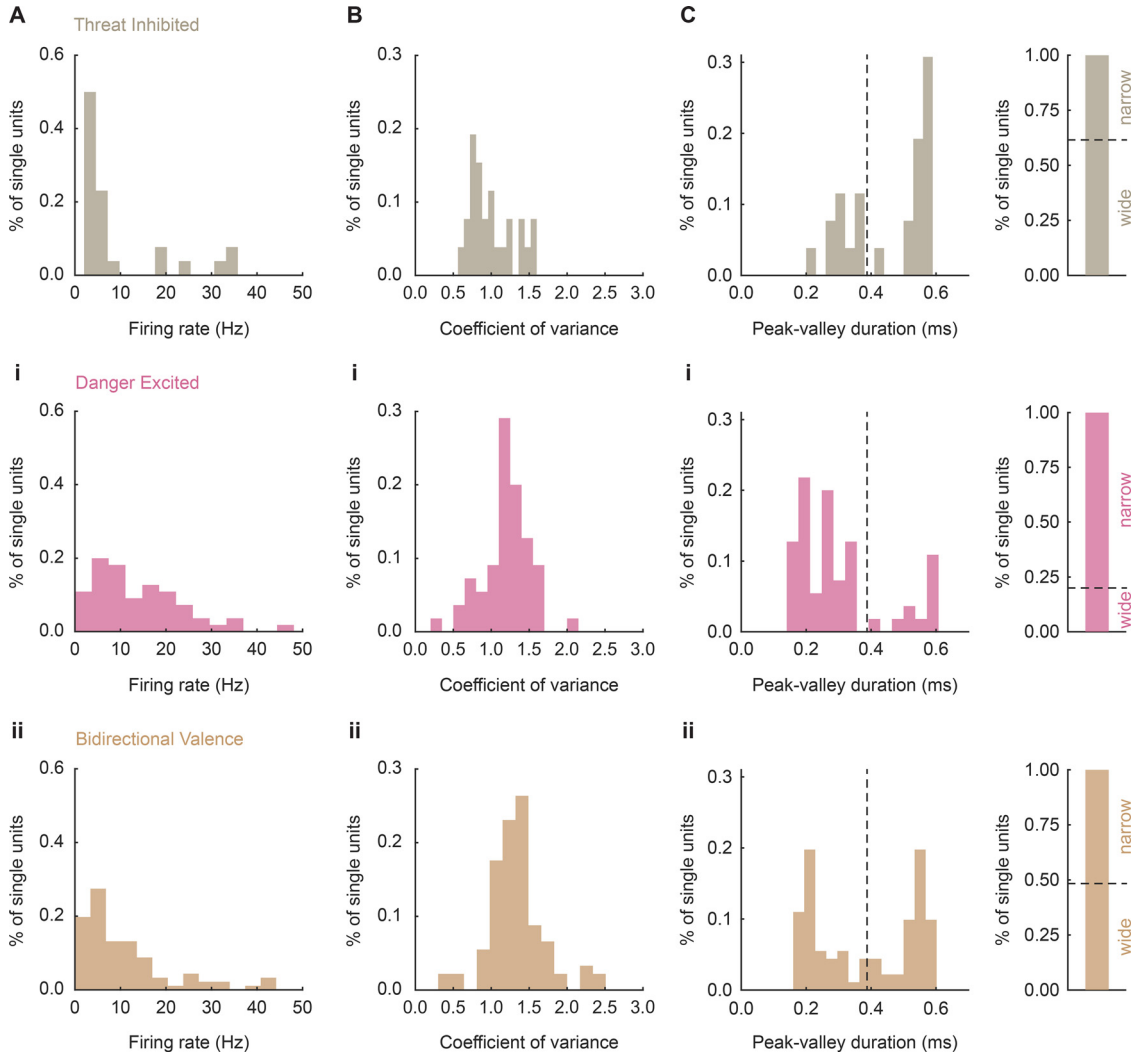

Figure 3. Firing and waveform characteristics of cue-responsive neurons. ***A***, ***i***, ***ii***, Histograms depict the distribution of the firing rate (in hertz, Hz) during a 10 s baseline period just before cue onset for Threat Inhibited ($n = 26$, gray), Danger Excited ($n = 55$, pink), and Bidirectional Valence ($n = 91$, tan) neurons. ***B***, ***i***, ***ii***, Identical graphs made for the coefficient of variance for Threat Inhibited, Danger Excited, and Bidirectional Valence neurons. ***C***, ***i***, ***ii***, Histogram (left) and bar graph (right) depicts the distribution of the waveform peak–valley duration (in milliseconds, ms) for Threat Inhibited, Danger Excited, and Bidirectional Valence neurons. Black dashed lines divide neurons into narrow (small values) and wide (large values) waveforms.

dorsal to the NAcc. Following recovery, single-unit activity was recorded during fear discrimination. At the conclusion of recording, rats were perfused, brains were sectioned, and electrode placements were confirmed with Nissl staining (Fig. 1*D*). Only placements within the NAcc, defined by a tear-shaped region surrounding the anterior commissure, were accepted (Fig. 1*E*).

A total of 368 NAcc single units were recorded from seven rats over 95 fear discrimination sessions. To identify cue-responsive single units in an unbiased manner, we compared the mean baseline firing rate (in hertz; 10 s before cue presentation) to the mean firing rate (in hertz) during the first 1 s and last 5 s of cue presentation. A single unit was considered cue responsive if it showed a significant firing change (increase or decrease) from baseline in response to danger, uncertainty, or safety during either the first 1 s or the last 5 s cue period (paired, two-tailed t test, $p < 0.05$). The first 1 s and last 5 s of cue presentation were selected because these time windows best captured NAcc firing patterns. This screen identified 193 cue-responsive single units (~53% of all units recorded) from 82 sessions, with at least seven cue-responsive single units identified in each rat (Extended Data Fig. 1-1).

Rats showed complete discrimination during the sessions in which cue-responsive single units were recorded (mean individual suppression ratio data are shown in Extended Data Fig. 1-1; session by session individual suppression ratio data are shown in Extended Data Fig. 1-2). Baseline nose poke rates were similar (Fig. 1*F*), and fear discrimination was observed across all seven rats (Fig. 1*G*). Suppression ratios were high in response to danger, intermediate in response to uncertainty, and low in response to safety. ANOVA for mean individual suppression ratio revealed a main effect of cue ($F_{(2,12)} = 57.41$, $p = 7.18 \times 10^{-7}$, $\eta_p^2 = 0.91$, op = 1.00). Suppression ratios differed for each cue pair. The 95% bootstrap confidence interval for differential suppression ratio did not contain zero for danger versus uncertainty [mean = 0.21; 95% CI, (lower bound) 0.16, (upper bound) 0.29], for uncertainty versus safety (mean = 0.47; 95% CI, 0.35, 1.03), and danger versus safety (mean = 0.69; 95% CI, 0.50, 1.25).

To reveal possible relationships between reward seeking and "fear," we examined relationships among individual baseline nose poke rate, cue suppression ratio (danger, uncertainty, safety), and overall discrimination (danger suppression ratio – safety suppression ratio; Fig. 1*H*). There was no relationship

between baseline nose poke rate and suppression in response to any cue or to overall discrimination (all $|R| < 0.73$, all $p > 0.06$). Discrimination was largely the product of reduced safety suppression ratios. In support, there was a significant negative relationship between overall discrimination and safety suppression ratio ($R = -0.98$, $p = 1.41 \times 10^{-4}$). Although fear was measured using conditioned suppression based on nose poke rates, the rate of baseline nose poking was unrelated to the degree to which cues suppressed nose poking.

NAcc neurons show heterogeneous cue firing

Single-unit firing patterns varied considerably, as did the direction and magnitude of their response. Firing heterogeneity indicated that NAcc single units could be divided into discrete, functional populations. To identify these populations, we summarized normalized firing rate in a 193 single unit × 6 epoch matrix. The six epochs were mean normalized firing rates taken from the first 1 s and last 5 s of danger, uncertainty, and safety presentation. We applied k-means clustering to the matrix and found that five clusters grouped similar functional types (Extended Data Fig. 2-1). To visualize firing patterns, we organized single units by cluster and plotted mean single-unit danger, uncertainty, safety, and reward firing (Fig. 2). The complete firing pattern of each cluster—considering cue and reward—led us to conclude that each functional population signaled a unique type of information: threat, danger, and Bidirectional Valence. Analyses are designed to systematically reveal these firing patterns.

Threat Excited neurons ($n = 5$; Fig. 2, row 1) and Threat Inhibited neurons ($n = 26$; Fig. 2, row 2) showed equivalent firing changes in response to danger and uncertainty, and lesser firing changes in response to safety. Danger Excited neurons ($n = 55$; Fig. 2, row 3) and Bidirectional Valence neurons ($n = 91$; Fig. 2, row 4) showed modest firing changes in response to danger, but lesser firing changes in response to uncertainty and safety. Non-Selective neurons ($n = 16$; Fig. 2, row 5) showed firing increases that did not differentiate the cues. Threat Excited neurons ($n = 5$) were observed in only two of seven subjects, with four single units coming from one subject. Thus, we are not confident that these single units are representative of the NAcc. Threat Inhibited neurons were obtained from four of seven subjects, Danger Excited neurons from six of seven subjects, and Bidirectional Valence neurons from all seven subjects. Our primary analyses focused on NAcc-representative populations showing differential cue firing ($n = 172$; Threat Inhibited, Danger Excited, and Bidirectional Valence neurons) and the fear discrimination sessions ($n = 79$) in which they were recorded.

We sought to determine whether Threat Inhibited, Danger Excited, and Bidirectional Valence neurons were likely composed of different neuron types. Previous studies have used baseline firing rate, coefficient of variance, and waveform peak–valley duration to distinguish NAcc medium spiny neurons (MSNs) from fast-spiking interneurons (FSIs; Berke et al., 2004; Berke, 2008; Gage, 2010; Yarom and Cohen, 2011; Sosa et al., 2020; Vachez, 2021). In our fear discrimination procedure, baseline firing rate was taken from a period when rats were poking for and consuming food rewards, making baseline firing rate and coefficient of variance poor indicators of firing at rest. Further, we observed unimodal distributions for baseline firing rate (Hartigan's Dip Statistic = 0.013, $p = 1.00$; Fig. 3*A*,*i*,*ii*) and coefficient of variance (Hartigan's Dip Statistic = 0.016, $p = 0.99$; Fig. 3*B*,*i*,*ii*) across all 172 neurons. We therefore focused on waveform peak–valley duration, which would be less contaminated by behavior (Fig. 3*C*,*i*,*ii*). Narrow waveforms are indicative of FSIs, while wide waveforms are indicative of projecting MSNs. Consistent with recordings coming from a mix of FSIs and MSNs, we observed a bimodal distribution for waveform peak–valley duration across all 172 neurons (Hartigan's Dip Statistic: test could not provide a specific p value, but instead returned 0.00). Single units tended to fall at the distribution extremes: narrow or wide waveforms. We then applied Hartigan's Dip Statistic to each population, determining whether it was primarily composed of narrow or wide waveforms, or a mix of both.

Wide waveforms, putative MSNs, were more common among Threat Inhibited neurons (Fig. 3*C*). A bimodal distribution, indicating a mix of MSNs and FSIs, was only detected if an uncorrected p value was used (Hartigan's Dip Statistic = 0.096, $p = 0.035$). Danger Excited neurons (Fig. 3*C*,*i*) showed a unimodal distribution (Hartigan's Dip Statistic = 0.06, $p = 0.18$), with most single units exhibiting narrow waveforms, typical of FSIs. Bidirectional Valence neurons (Fig. 3*C*,*ii*) showed a bimodal distribution (Hartigan's Dip Statistic = 0.11, $p = 0.00$; test could not provide specific p value), with an approximately 50/50 split between narrow and wide waveforms (a mix of putative FSIs and MSNs). Single-unit function is likely related to neuron type (an observation we return to in the Discussion).

NAcc populations show distinct danger and uncertainty firing patterns

Having uncovered distinct NAcc functional populations, we sought to reveal the specific cue firing patterns of each. For each population, we performed ANOVA for normalized firing rate [factors: cue (danger, uncertainty, safety) and interval (250 ms bins, from 2 s before cue onset to cue offset)]. Confirming differential firing, ANOVA for Threat Inhibited neurons ($n = 26$) revealed a main effect of cue ($F_{(2,50)} = 37.84$, $p = 9.83 \times 10^{-11}$, $\eta_p^2 = 0.60$, op = 1.00), interval ($F_{(47,1175)} = 11.51$, $p = 8.23 \times 10^{-68}$, $\eta_p^2 = 0.32$, op = 1.00), and a significant cue × interval interaction ($F_{(94,2350)} = 4.95$, $p = 7.61 \times 10^{-45}$, $\eta_p^2 = 0.17$, op = 1.00). Population activity suggests equivalent firing decreases in response to danger and uncertainty that exceeded firing decreases in response to safety (Fig. 4*A*). In support, Threat Inhibited neurons showed greater firing decreases in response to threat cues (danger and uncertainty) compared with safety at onset (mean = −0.47; 95% CI, −0.63, −0.32; Fig. 4*B*, left), and during late cue (mean = −0.44; 95% CI, −0.60, −0.20; Fig. 4*B*, right). Firing decreases in response to danger and uncertainty did not differ at onset (mean = −0.01; 95% CI, −0.11, 0.12) or during late cue (mean = −0.02; 95% CI, −0.14, 0.12). Threat-inhibited neurons showed equivalent firing decreases in response to danger and uncertainty that exceeded those in response to safety throughout cue presentation.

Confirming differential cue firing for Danger Excited neurons ($n = 55$; Fig. 4*C*), ANOVA revealed a main effect of cue ($F_{(2,106)} = 13.05$, $p = 9.00 \times 10^{-6}$, $\eta_p^2 = 0.20$, op = 1.00) and interval ($F_{(47,2491)} = 7.12$, $p = 1.17 \times 10^{-41}$, $\eta_p^2 = 0.12$, op = 1.00), and a significant cue × interval interaction ($F_{(94,4982)} = 2.23$, $p = 1.87 \times 10^{-10}$, $\eta_p^2 = 0.04$, op = 1.00). Firing was maximal in response to danger and fully discriminated the three cues at onset (danger vs uncertainty: mean = 0.22; 95% CI, 0.11, 0.33; uncertainty vs safety: mean = 0.21; 95% CI, 0.07, 0.33; Fig. 4*D*, left). As cue presentation proceeded, firing increases were selective in response to danger, whereas uncertainty and safety firing were minimal and equivalent. In support, Danger Excited neurons showed differential firing in response to danger compared with the mean of uncertainty and safety during late cue presentation (mean = 0.17; 95% CI, 0.07, 0.27; Fig. 4*D*, right). Danger Excited neuronal

firing initially discriminated all cues before becoming specific to the danger cue.

Bidirectional Valence neurons ($n = 91$) were the most abundant functional type, accounting for ~47% of cue-responsive NAcc neurons. To reveal whether these neurons also showed differential firing that was more specific to danger, we first performed ANOVA. Confirming differential firing (Fig. 4*E*), ANOVA revealed a significant main effect of cue ($F_{(2,178)} = 8.90$, $p = 2.07 \times 10^{-4}$, $\eta_p^2 = 0.09$, op = 0.97), interval ($F_{(47,4183)} = 3.98$, $p = 4.49 \times 10^{-18}$, $\eta_p^2 = 0.04$, op = 1.00), and a significant cue × interval interaction ($F_{(94,8366)} = 1.45$, $p = 0.003$, $\eta_p^2 = 0.02$, op = 1.00). Confirming more selective danger firing, Bidirectional Valence neurons showed danger firing decreases that exceeded uncertainty and safety decreases at onset (mean = −0.13; 95% CI, −0.22, −0.03; Fig. 4*F*, left), as well as late cue (mean = −0.09; 95% CI, −0.16, −0.02; Fig. 4*F*, right).

As a population, Bidirectional Valence neurons showed minimal safety firing. However, inspection of the single units (Fig. 4*F*, left) revealed considerable variation in safety onset firing, with some neurons showing large safety firing increases. There was greater variability in onset safety firing compared with either danger (Pitman–Morgan test, $p = 0.0087$) or uncertainty onset firing (Pitman–Morgan test, $p = 0.0046$). Bidirectional Valence neuronal firing distinguished danger from uncertainty and safety throughout cue presentation, though neurons varied in their safety onset firing.

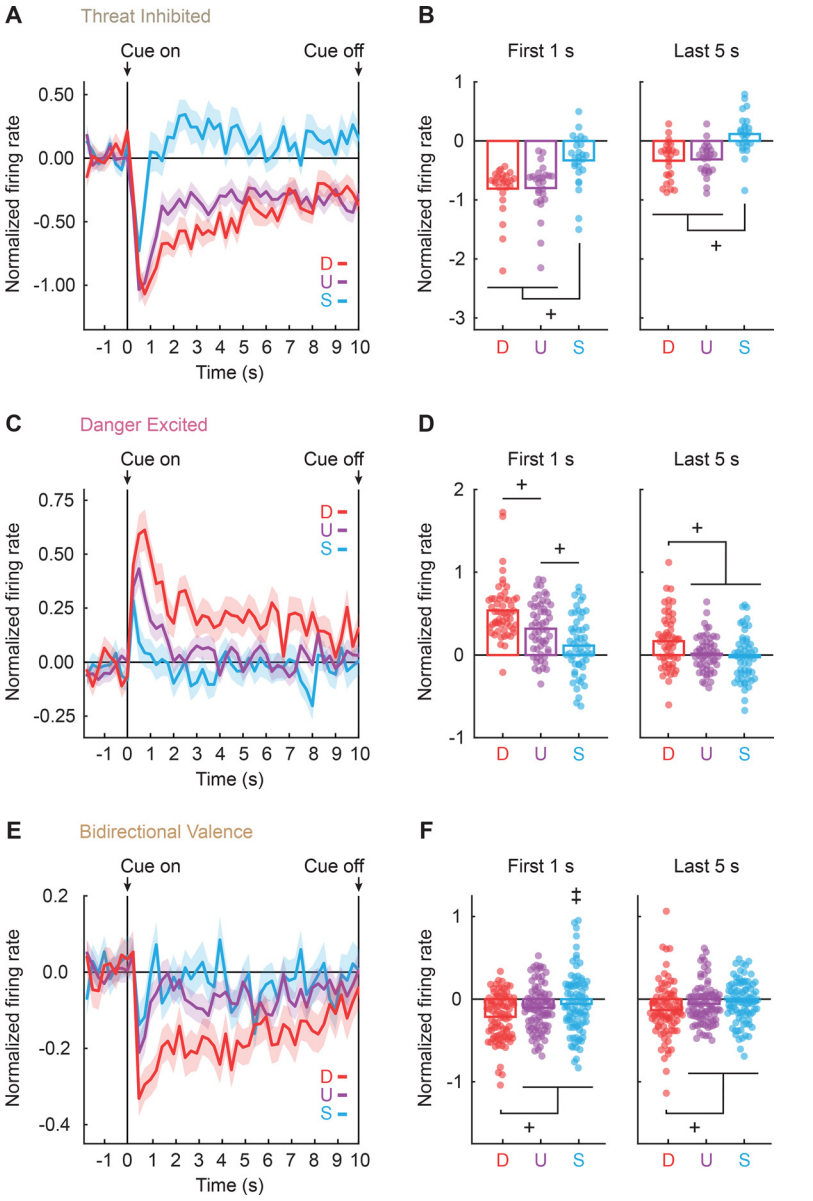

Figure 4. Differential firing by cue-responsive neurons. ***A***, Mean normalized firing rate to danger (D; red), uncertainty (U; purple), and safety (S; blue) is shown from 2 s before cue onset to cue offset for the Threat Inhibited neurons ($n = 26$, gray). Cue onset and offset are indicated by vertical black lines. SEM is indicated by shading. ***B***, Mean (bar) and individual (data points) normalized firing rate for Threat Inhibited neurons during onset (the first 1 s cue, left) and late cue (the last 5 s cue, right) are shown for each cue (D, U, S). Colors maintained from ***A***. ***C–F***, Identical graphs made for Danger Excited ($n = 55$, pink) and Bidirectional Valence neurons ($n = 91$, tan), as in ***A*** and ***B***. $^{+}$95% bootstrap confidence interval for differential cue firing does not contain zero; ‡Pitman–Morgan test, $p < 0.05$.

Threat Excited and Non-Selective population

Though not our focus, we show complete firing for Threat Excited and Non-Selective neurons (Fig. 5). ANOVA for Threat Excited neurons ($n = 5$) revealed a main effect of interval ($F_{(47,188)} = 19.75$, $p = 1.99 \times 10^{-51}$, $\eta_p^2 = 0.83$, op = 1.00) and a significant cue × interval interaction ($F_{(94,376)} = 1.46$, $p = 0.008$, $\eta_p^2 = 0.27$, op = 1.00). Threat Excited neurons (Fig. 5*A*) showed greater firing increases to threat cues (danger and uncertainty) compared with safety at onset (mean = 0.90; 95% CI, 0.30, 12.58; Fig. 5*B*, left), but not during late cue (mean = 0.39; 95% CI, −1.08, 1.11; Fig. 5*B*, right). ANOVA for Non-Selective neurons (Fig. 5*C*) found neither a main effect of cue ($F_{(2,30)} = 3.04$, $p = 0.063$, $\eta_p^2 = 0.17$, op = 0.55) nor a cue × interval interaction ($F_{(94,1410)} = 1.19$, $p = 0.11$, $\eta_p^2 = 0.07$, op = 1.00). Nonselective firing increases in response to threat cues (danger and uncertainty) did not differ from safety at onset (mean = 0.07; 95% CI, −0.22, 0.36; Fig. 5*D*, left), or during late cue (mean = 0.17; 95% CI, −0.09, 0.46; Fig. 5*D*, right).

Threat Inhibited neurons show greatest temporal firing similarity

Previous analyses reveal that Threat Inhibited neurons fire more similarly in response to danger and uncertainty than Danger Excited and Bidirectional Valence neurons. Perhaps Threat Inhibited neurons also show more similar temporal firing patterns in response to danger and uncertainty over cue presentation. Inspired by representational similarity analyses (Kriegeskorte et al., 2008; Ritchey et al., 2013), we devised a firing similarity analysis. To do this, we divided the mean normalized firing rate for each cue into 12, 1 s bins (2 s before cue onset through 10 s cue presentation). We correlated the normalized firing rate over this 12 s period for each neuron–cue pair using Pearson's correlation coefficient. The firing similarity for each population was determined using the *R* value for each neuron–cue pair (Fig. 6*A–C*).

Threat Inhibited neurons showed the greatest firing similarity in response to danger and uncertainty (Fig. 6*D*). Danger/uncertainty firing similarity exceeded the similarity for uncertainty/

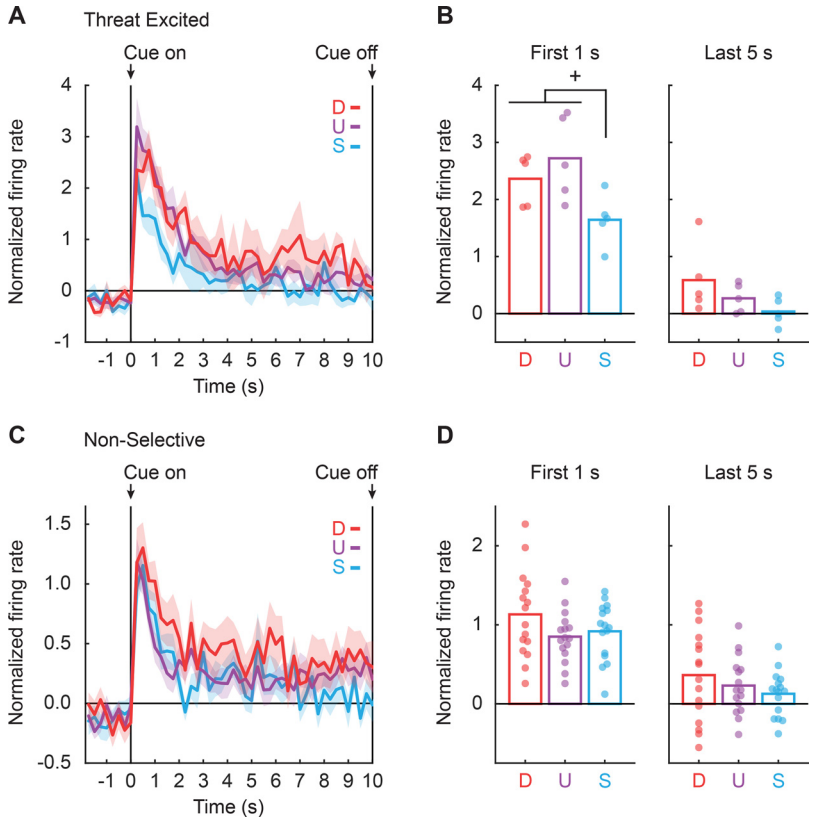

Figure 5. Threat Excited and Non-Selective NAcc neuron firing. ***A***, Mean normalized firing rate in response to danger (D; red), uncertainty (U; purple), and safety (S; blue) is shown from 2 s before cue onset to cue offset for the Threat Excited neurons ($n = 5$). Cue onset and offset are indicated by vertical black lines. SEM is indicated by shading. ***B***, Mean (bar) and individual (data points), normalized firing rate for Threat Excited neurons during onset (the first 1 s cue, left) and late cue (the last 5 s cue, right) are shown for each cue (D, U, S). Colors are as in ***A***. ***C***, ***D***, Identical graphs made for Non-Selective neurons ($n = 16$), as in ***A*** and ***B***. $^{+}$95% bootstrap confidence interval for differential cue firing does not contain zero.

safety and danger/safety. Further, danger/uncertainty firing similarity by Threat Inhibited neurons exceeded that for Danger Excited (Fig. 6*E*) and Bidirectional Valence neurons (Fig. 6*F*). In support, ANOVA for *R* value [factors: population (Threat Inhibited, Danger Excited, Bidirectional Valence) and comparison (danger vs uncertainty, uncertainty vs safety, and danger vs safety)] revealed significant main effects of population ($F_{(2,169)}$= 3.34, $p = 0.038$, $\eta_p^2 = 0.04$, op = 0.63) and comparison ($F_{(2,338)}$= 26.26, $p = 2.51 \times 10^{-11}$, $\eta_p^2 = 0.13$, op = 1.00), but critically a significant population × comparison interaction ($F_{(4,338)}$= 3.86, $p = 0.004$, $\eta_p^2 = 0.04$, op = 0.90). Paired *t* tests (Bonferroni corrected for nine tests; 0.05/9 = 0.0056) revealed Threat Inhibited *R* values for danger/uncertainty to exceed those for uncertainty/safety ($t_{(25)} = 3.31$, $p = 0.003$), and danger/safety ($t_{(25)} = 4.11$, $p = 3.74 \times 10^{-4}$). Danger Excited *R* values for danger/uncertainty exceed those for uncertainty/safety ($t_{(54)} = 3.24$, $p = 0.002$) and danger/safety ($t_{(54)} = 4.21$, $p = 9.60 \times 10^{-5}$), but no differences were observed for any cue pair in Bidirectional Valence neurons (all *t* values < 2.1, all *p* values > 0.0056). Across all populations and cue pairs, the greatest firing similarity was observed in response to the danger and uncertainty cues generated by Threat Inhibited neurons.

NAcc neurons do not signal fear output

NAcc neurons are known to alter firing around reward seeking (Janak et al., 2004). It is therefore possible that observed danger and uncertainty firing reflects nose poke suppression. In other words, NAcc neurons may signal fear output, not threat information. First, to determine the cue firing pattern best describing each population, we used linear regression to construct a tuning curve. For each single unit, we calculated the mean normalized firing rate for each 10 s cue (16 total: 4 danger, 8 uncertainty, and 4 safety trials). The cue firing pattern regressor consisted of a numerical value assigned to each cue. The values assigned to danger (1.00) and safety (0.00) were fixed, reflecting the shock probability assigned to each cue. The value assigned to uncertainty was incremented from 0 to 1 in 0.25 steps (0.00, 0.25, 0.50, 0.75, 1.00). Regression was separately performed for each of the five uncertainty assignments. Regression output was a beta coefficient, quantifying the strength (greater distance from 0 = stronger) and direction (>0 = positive; <0 = negative) of the predictive relationship between each cue firing pattern regressor and single-unit firing. A tuning curve was constructed by averaging beta coefficients across the 10 s cue for each cue firing pattern regressor at each uncertainty assignment. The extreme of the Threat Inhibited tuning curve occurred at an uncertainty assignment of 0.75, while the extremes of the tuning curves for Danger Excited and Bidirectional Valence neurons occurred at an uncertainty assignment of 0.50 (Fig. 7). Thus, the specific cue firing pattern for each population constituted an exaggerated threat signal that did not reflect the actual footshock probability assigned to uncertainty (0.25).

Next, we used linear regression to determine the degree to which single-unit firing reflected fear output versus exaggerated threat over cue presentation. For each single unit, we calculated the normalized firing rate for each trial in 1 s bins from 2 s before cue onset through 10 s cue presentation. The fear output regressor was the cue suppression ratio for that specific trial. The exaggerated threat regressor was the cue firing pattern specific to the population. To determine the time course of fear output and exaggerated threat signaling, we performed ANOVA for beta coefficients [factors: regressor (fear output and exaggerated threat) and interval (1 s bins, from 2 s before cue onset to cue offset)].

Each NAcc population signaled exaggerated threat, but not fear output. Exaggerated threat signaling was strongest during early cue presentation. In support, ANOVA for Threat Inhibited neurons (Fig. 8*A*) found a regressor × interval interaction ($F_{(11,264)} = 2.32$, $p = 0.01$, $\eta p^2 = 0.09$, op = 0.95). Beta coefficients for exaggerated threat, but not for the fear output, were shifted below zero during early cue (mean = −0.97; 95% CI, −1.42, −0.56) and late cue (mean = −0.47; 95% CI, −0.86, −0.05; Fig. 8*B*). Exaggerated threat and fear output beta coefficients differed during early cue (mean = −0.92; 95% CI, −1.58, −0.32, but not during late cue (mean = −0.36; 95% CI, −1.06, 0.43; Fig. 8*B*). ANOVA for Danger Excited neurons (Fig. 8*C*) found a main effect of regressor ($F_{(1,53)} = 6.64$, $p = 0.01$, $\eta p^2 = 0.11$, op = 0.72). Beta coefficients exceeding zero were observed for exaggerated threat during early cue (mean = 0.43; 95% CI, 0.22, 0.61), as well as late cue (mean = 0.30; 95% CI, 0.06, 0.51), but not for the fear

output (Fig. 8*D*). Exaggerated threat and fear output beta coefficients differed during early cue (mean = 0.39; 95% CI, 0.10, 0.69), but not during the late cue (mean = 0.29; 95% CI, −0.05, 0.58; Fig. 8*D*). ANOVA for Bidirectional Valence neurons (Fig. 8*E*) revealed a main effect of regressor ($F_{(1,85)} = 6.22$, $p = 0.015$, $\eta p^2 = 0.07$, op = 0.69) and a regressor × interval interaction ($F_{(11,935)} = 2.56$, $p = 0.003$, $\eta p^2 = 0.03$, op = 0.97). Early beta coefficients were shifted below zero for exaggerated threat (mean = −0.31; 95% CI, −0.45, −0.16), but not for fear output (mean = 0.08; 95% CI, −0.05, 0.20; Fig. 8*F*). Exaggerated threat and fear output beta coefficients differed during early cue (mean = −0.39; 95% CI, −0.62, −0.12), but not during the late cue (mean = −0.16; 95% CI, −0.40, 0.08; Fig. 8*F*).

Reward-related firing confirms NAcc threat and Bidirectional Valence populations

The goal of the current study was to examine NAcc firing to threat and safety cues. While our procedure was optimized to assess threat cue firing, the use of conditioned suppression permitted us to record activity around reward delivery. To determine whether our cue-responsive neurons showed reward-related firing, we aligned the firing of our three main populations (Threat Inhibited, Danger Excited, Bidirectional Valence) to pellet feeder advance (Fig. 9*A*). Activity was sampled around rewards delivered during the intertrial interval, avoiding contamination by cue and footshock deliveries.

We performed ANOVA for normalized firing rate [factors: population (Threat Inhibited, Danger Excited, Bidirectional Valence) and interval (16, 250 ms bins: 2 s before and 2 s following pellet feeder advance)]. ANOVA revealed a main effect of interval ($F_{(15,2430)} = 3.83$, $p = 8.49 \times 10^{-7}$, $\eta_p^2 = 0.02$, op = 1.00), but more critically, a population × interval interaction ($F_{(30,2430)} = 1.72$, $p = 0.009$, $\eta_p^2 = 0.02$, op = 1.00). The interaction was the result of Bidirectional Valence neurons selectively increasing firing following pellet feeder advance. ANOVA restricted to Bidirectional Valence neurons found a main effect of interval ($F_{(15,1290)} = 8.78$, $p = 1.24 \times 10^{-19}$, $\eta_p^2 = 0.09$, op = 1.00), while separate ANOVA for Threat Inhibited and Danger Excited neurons found no main effects of interval ($F < 1.1$, $p > 0.4$). Population firing patterns were evident in single units (Fig. 9*B–D*). In Threat Inhibited and Danger Excited neurons, pre-reward and post-reward firing differed neither from zero nor from each other (all 95% CIs contained zero; Fig. 9*B*,*C*). By contrast, Bidirectional Valence firing around zero before reward (mean = 0.04; 95% CI, −0.07, 0.13) gave way to firing increases post-reward (mean = 0.47; 95% CI, 0.28, 0.62), and post-reward firing exceeded pre-reward firing (mean = 0.42; 95% CI, 0.21, 0.58; Fig. 9*D*).

Bidirectional Valence neurons, which increased firing following pellet feeder advance, sustained firing decreases to danger, and showed variable firing increases to safety onset, may generally signal valence. If this were the case, positive firing relationships would be observed for safety onset (first 1 s cue) and reward onset (first 250 ms following feeder advance); and negative firing relationships would be observed for danger (10 s cue) and reward onset (first 250 ms following feeder advance). Threat Inhibited neurons (Fig. 9*E*) showed a non-significant, negative firing relationship between reward onset firing and safety onset firing ($R^2 = 0.07$, $p = 0.18$), a significant, negative firing relationship between reward onset firing and danger firing ($R^2 = 0.15$, $p = 0.05$), and these two correlations did not differ ($Z = -0.50$, $p = 0.62$). Danger Excited neurons (Fig. 9*F*) showed a non-significant positive firing relationship between reward onset firing and safety onset firing ($R^2 = 0.06$, $p = 0.07$), a non-significant, negative firing relationship between reward onset firing and danger firing ($R^2 = 0.06$, $p = 0.07$), but these two correlations differed ($Z = -2.10$,

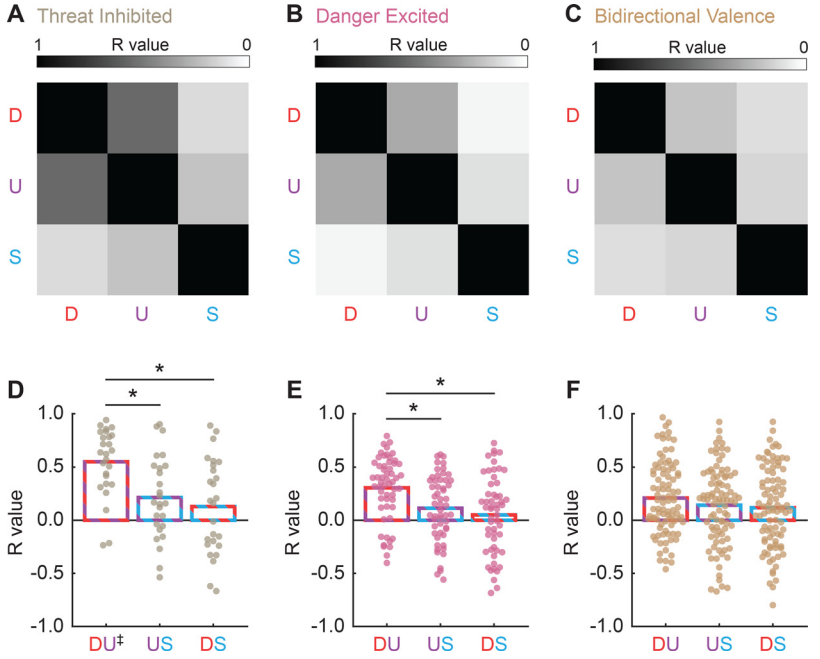

Figure 6. Temporal firing similarity by cue-responsive neurons. ***A–C***, Firing similarity matrices between cue pairs [D, danger (red); U, uncertainty (purple); S, safety (blue)] are depicted for Threat Inhibited ($n = 26$, gray; ***A***), Danger Excited ($n = 55$, pink; ***B***), and Bidirectional Valence ($n = 91$, tan; ***C***) neurons. Color scale for correlation coefficient (R) is shown, with the greatest firing similarities shown in black ($R = 1$) and the least firing similarities shown in white ($R = 0$). ***D–F***, Mean (bar) and individual (data points) correlation coefficients (R): danger versus uncertainty (DU), uncertainty versus safety (US), and danger versus safety (DS) are shown for each population. *Bonferroni t test, $p < 0.05$; ‡unpaired t test, $p < 0.05$.

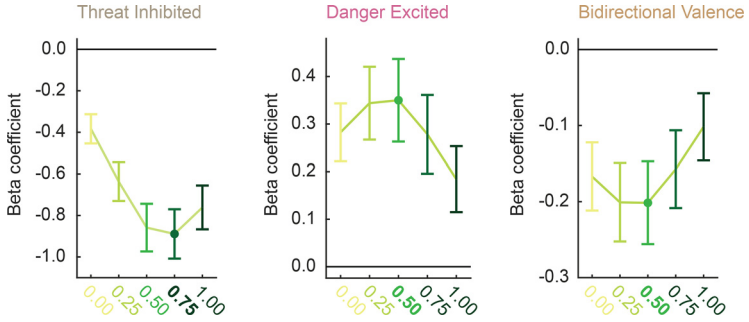

Figure 7. NAcc tuning curves. Mean ± SEM beta coefficients are shown for cue pattern regressor, during the 10 s cue presentation, for each uncertainty assignment from 0 to 1 in 0.25 increments (0.00, 0.25, 0.50, 0.75, 1.00), for the Threat Inhibited ($n = 26$, left), Danger Excited ($n = 55$, middle), and Bidirectional Valence ($n = 91$, right) neurons.

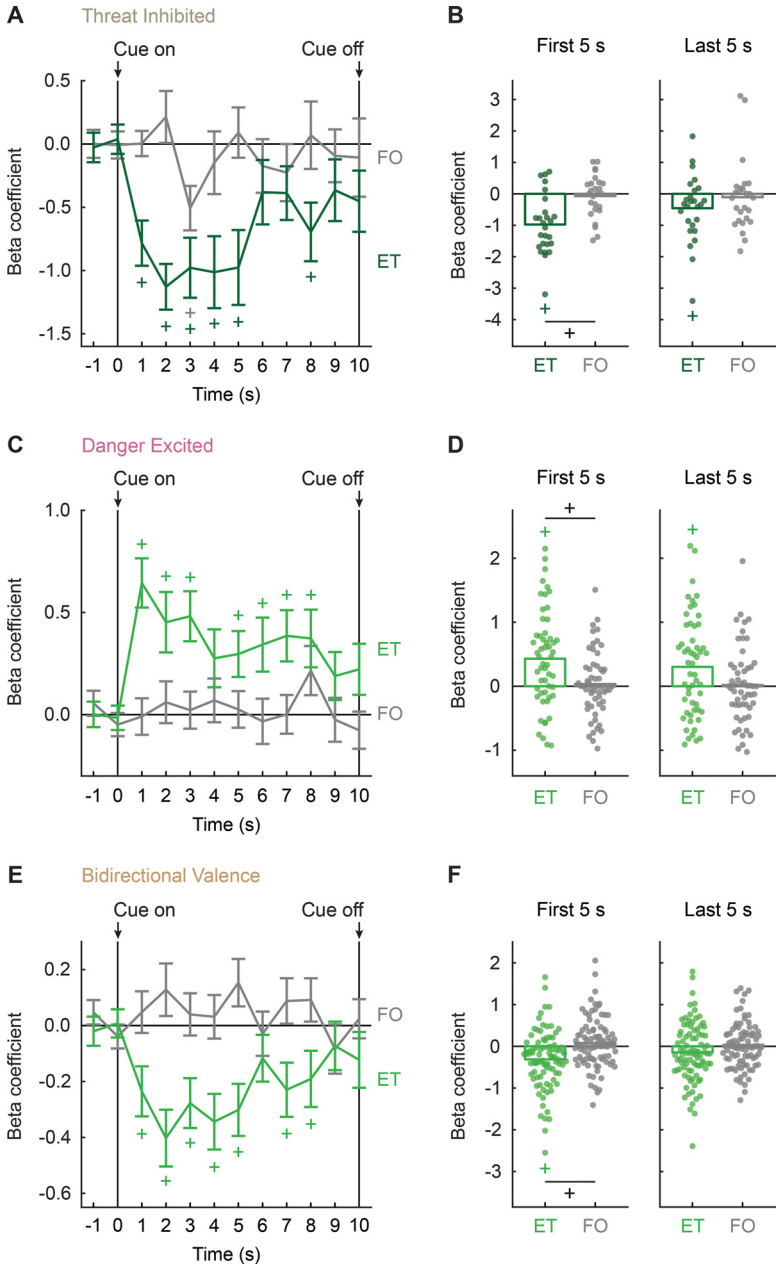

Figure 8. NAcc neurons do not signal fear output. ***A***, Mean ± SEM beta coefficients are shown for each regressor [ET, exaggerated threat (dark green); FO, fear output (gray)], from 2 s before cue onset to cue offset in 1 s intervals for the Threat Inhibited neurons ($n = 26$). Cue onset and offset are indicated by vertical black lines. ***B***, Mean (bar) and individual (data points) early cue (the first 5 s cue, left) and late cue (the last 5 s cue, right) beta coefficients for each regressor (ET and FO) are shown for Threat Inhibited neurons (colors are as in ***A***). ***C–F***, Identical graph made for the Danger Excited neurons ($n = 55$) and Bidirectional Valence neurons ($n = 91$), as in ***A*** and ***B***. $^{+}$95% bootstrap confidence interval for differential beta coefficient does not contain zero. $^{+}$95% bootstrap confidence interval for beta coefficient does not contain zero (colored + signs).

$p = 0.035$). Thus, neither Threat Inhibited nor Danger Excited neurons are strong candidates for valence signaling.

Bidirectional Valence neurons (Fig. 9*G*) showed a significant, positive relationship between reward onset firing and safety onset firing ($R^2 = 0.08$, $p = 0.006$); a significant, negative relationship between reward onset firing and danger firing ($R^2 = 0.12$, $p = 8.43 \times 10^{-4}$); and these two correlations significantly differed ($Z = -3.96$, $p = 7.70 \times 10^{-5}$). If neurons signal valence, opposing firing changes should be observed to safety onset firing and danger firing. While Threat Inhibited neurons ($R^2 = 0.06$, $p = 0.24$; Fig. 9*H*) showed zero firing relationship, Danger Excited neurons ($R^2 = 0.25$, $p = 1.17 \times 10^{-4}$; Fig. 9*I*) and Bidirectional Valence neurons ($R^2 = 0.06$, $p = 0.015$; Fig. 9*J*) showed significant, negative firing relationships. The results reveal selective threat signaling by Threat Inhibited neurons, somewhat ambiguous signaling by Danger Excited neurons, and valence signaling by Bidirectional Valence neurons.

Finally, NAcc populations showed minimal firing changes around periods of natural nose poke cessation occurring during the intertrial intervals, when no cues or footshocks were presented (Fig. 10*A*). ANOVA for normalized firing rate [factors: population (Threat Inhibited, Danger Excited, Bidirectional Valence) and interval (16, 250 ms bins: 2 s before and 2 s following nose poke cessation)] found no main effect of interval ($F_{(15,2535)} = 1.58$, $p = 0.071$, $\eta_p^2 = 0.01$, op = 0.90), but did find a population × interval interaction ($F_{(30,2535)} = 2.18$, $p = 2.35 \times 10^{-4}$, $\eta_p^2 = 0.03$, op = 1.00). The interaction was driven by modest Bidirectional Valence firing increases both before and after nose poke cessation. In support, pre- and post-nose poke cessation firing differed neither from zero nor from each other for Threat Inhibited and Danger Excited neurons (all 95% CIs contained 0; Fig. 10*B*,*C*). Pre- and post-nose poke cessation firing both exceeded zero, but did not differ from each other for Bidirectional Valence neurons (Fig. 10*D*). Finally, zero relationships were observed between nose poke cessation (first 250 ms following nose poke cessation) and cue firing (safety onset, first 1 s cue; danger, 10 s cue) for the three main populations (all R^2 values < 0.02, all p values > 0.45; Fig. 10*E–G*). Thus, NAcc cue firing reflects cue information, not the resultant suppression of nose poking.

Discussion

We recorded NAcc single-unit activity while female rats discriminated danger, uncertainty, and safety cues. Demonstrating threat firing, most NAcc neurons showed the greatest firing changes in response to the shock-associated cues: danger and uncertainty. Heterogeneity in cue and reward firing led us to identify distinct functional types. Danger Excited neurons preferentially increased firing to the danger cue and were unresponsive to reward. Threat Inhibited neurons decreased firing to danger and uncertainty cues, and were also unresponsive to reward. Bidirectional Valence neurons decreased firing in response to the danger cue (negative valence) and increased firing in response to reward delivery (positive valence).

Before discussing the organization of danger, threat, and valence signaling within the NAcc and its relationship to a larger network, several limitations should be noted. Our recordings came exclusively from female rats. NAcc activity and function

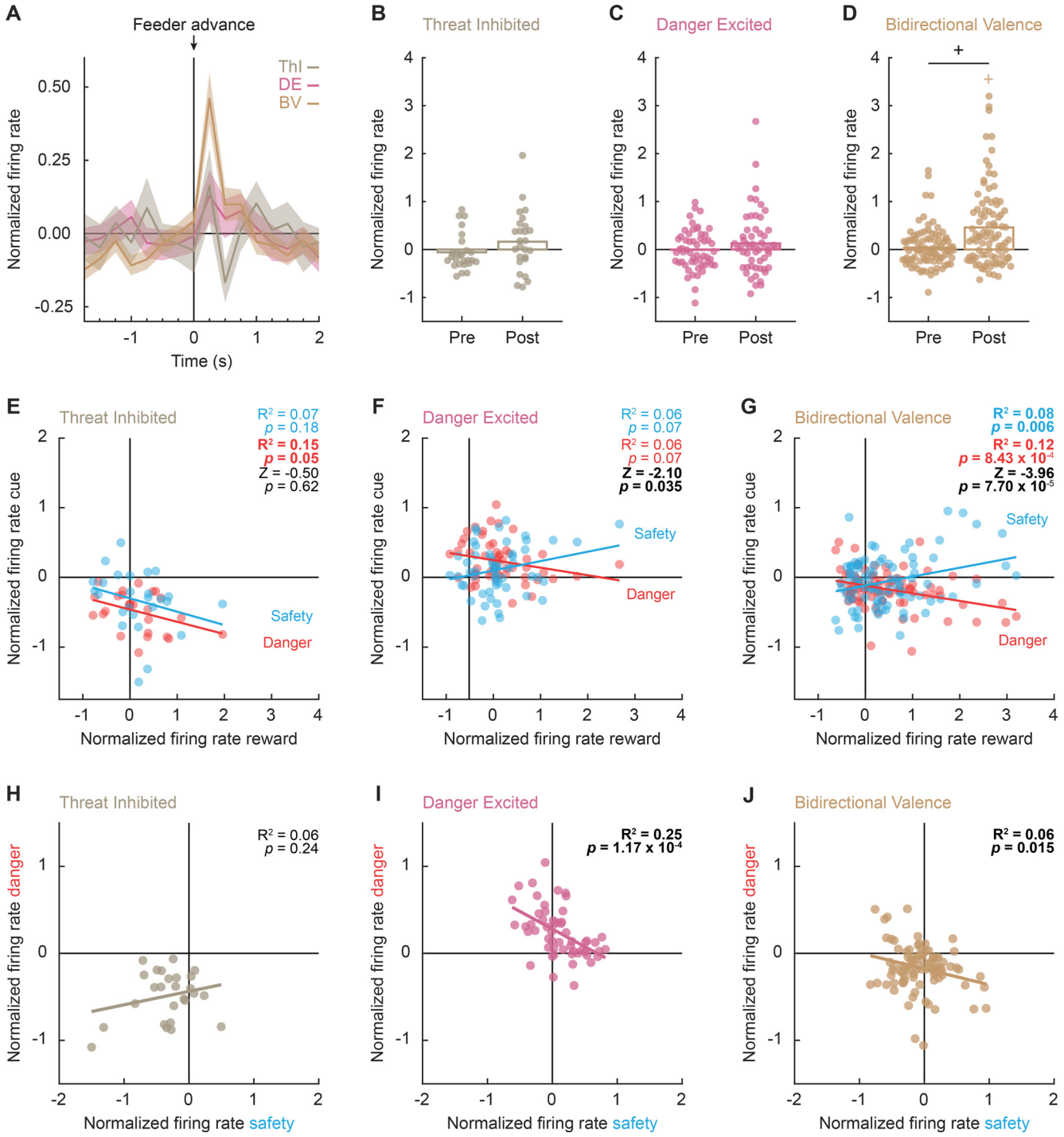

Figure 9. Reward firing by cue-responsive neurons. ***A***, Mean ± SEM normalized firing rate to reward is shown 2 s before and 2 s after reward delivery (advancement of feeder) for the Threat Inhibited ($n = 26$, gray), Danger Excited ($n = 55$, pink), and Bidirectional Valence neurons ($n = 91$, tan) neurons. Reward-related firing was extracted from intertrial intervals when no cues or footshocks were presented. Feeder advance is indicated by the black arrow. SEM is indicated by shading. ***B–D***, Mean (bar) and individual (data points) normalized firing rates for Threat Inhibited (***B***), Danger Excited (***C***), and Bidirectional Valence (***D***) neurons are shown during the 250 ms interval prior (pre) to and 250 ms interval after (post) reward delivery. $^{+}$95% bootstrap confidence interval for differential reward firing does not contain zero. $^{+}$95% bootstrap confidence interval for normalized firing rate does not contain zero (colored + sign). ***E–G***, Mean normalized firing rate to cues (danger, 10 s cue, red; safety, the first 1 s cue, blue) versus reward is plotted for Threat Inhibited (***E***), Danger Excited (***F***), and Bidirectional Valence (***G***) neurons. ***H–J***, Mean normalized firing rate to danger (10 s cue) versus safety (the first 1 s cue) is plotted for Threat Inhibited (***H***), Danger Excited (***I***), and Bidirectional Valence (***J***) neurons. Trendline, the square of the Pearson correlation coefficient (R^2) and associated p value are shown. Fisher r-to-z transformations (Z) are shown. Colors are as in ***A***.

have been reported to be similar across sexes (Lobo et al., 2010; Cole et al., 2018; Gold et al., 2019; Soares-Cunha et al., 2020; Strong et al., 2020). Previous studies from our laboratory have found complete and comparable fear discrimination in females and males (Walker et al., 2018, 2019). Nevertheless, we cannot rule out the possibility that NAcc threat/reward signaling may meaningfully differ by sex. Another consideration is that our behavioral design did not manipulate reward with the same nuance as threat. A behavioral procedure in which 5^{+} cues predict unique shock and reward probabilities would be necessary to

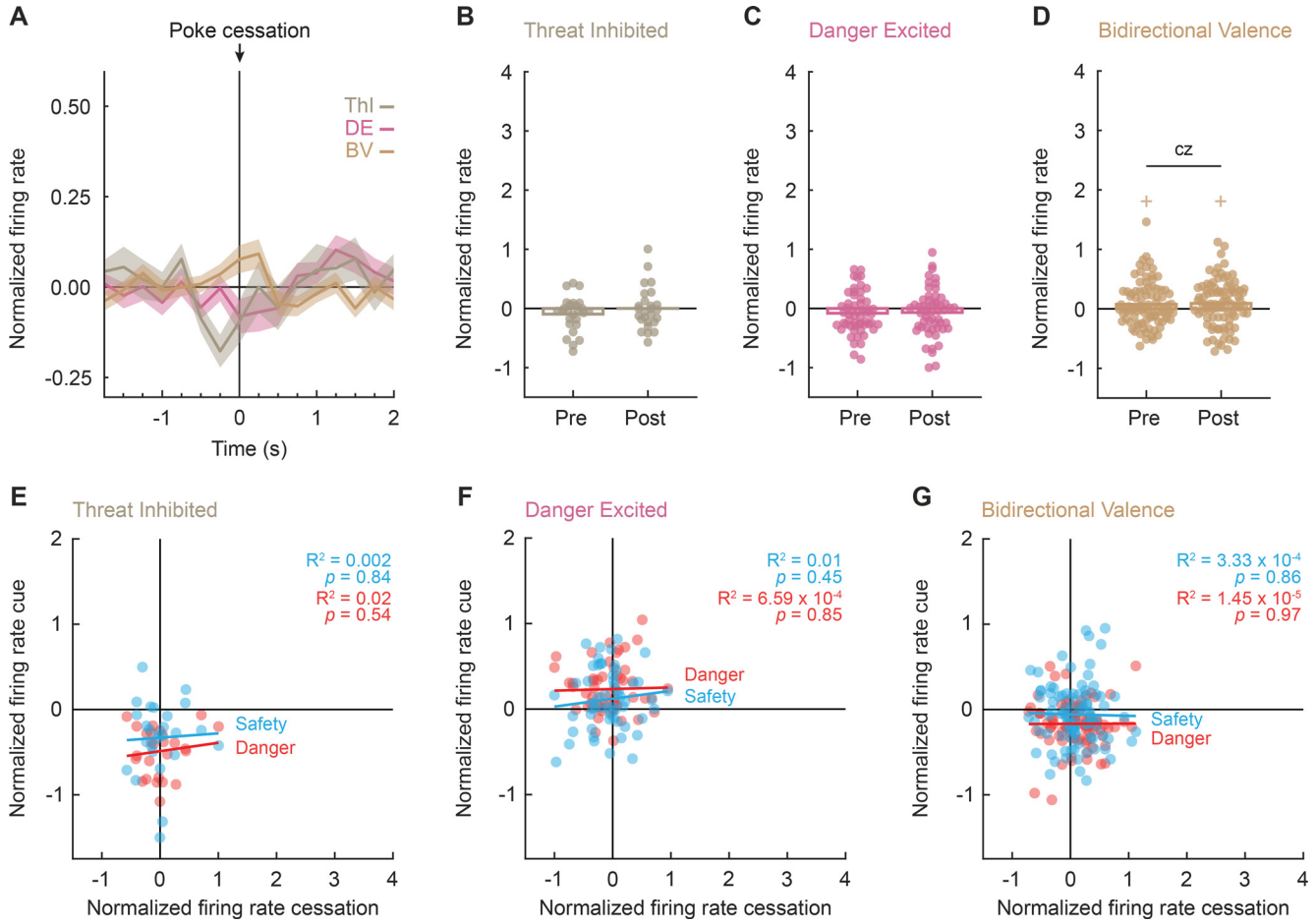

Figure 10. NAcc neurons are not responsive to nose poke cessation. ***A***, Mean ± SEM normalized firing rate is shown 2 s before and 2 s after nose poke cessation for the Threat Inhibited (Thl; $n = 26$; gray), Danger Excited (DE; $n = 55$; pink), and Bidirectional Valence (BV; $n = 91$; tan) neurons. Nose poke cessation is indicated by the black arrow. SEM is indicated by shading. ***B–D***, Mean (bar) and individual (data points) normalized firing rates for Threat Inhibited (***B***), Danger Excited (***C***), and Bidirectional Valence (***D***) neurons are shown during the 250 ms interval prior (pre) to and 250 ms interval after (post) nose poke cessation. ***E–G***, Mean normalized firing rate in response to cues (danger, 10 s cue, red; safety, the first 1 s cue, blue) versus nose poke cessation is plotted for Threat Inhibited ($n = 26$, gray; ***E***), Danger Excited ($n = 55$, pink; ***F***), and Bidirectional Valence ($n = 91$, tan; ***G***) neurons. Trendline, the square of the Pearson correlation coefficient (R^2) and associated p value are shown. ^{cz}95% confidence interval contains zero.

demonstrate complete Bidirectional Valence signaling by NAcc neurons.

Consistent with prior studies (Berke, 2008; Gage et al., 2010; Lansink et al., 2010; Sosa et al., 2020; Vachez et al., 2021), we found that waveform peak–valley duration was bimodally distributed in cue-responsive NAcc neurons. Narrow waveforms are consistent with FSIs, reflecting firing information confined within the NAcc. Wide waveforms are consistent with MSNs, the principal output neurons of the NAcc. Although one might expect tight coupling of FSI and MSN firing patterns *in vivo*, this has not been consistently observed (Lansink et al., 2010; Berke, 2011). Instead, FSI firing is often idiosyncratic and unrelated to neighboring neurons. We found that the Danger Excited population was primarily composed of putative FSIs, suggesting preferential danger processing within the NAcc. However, putative FSIs were also observed in the Threat Inhibited and Bidirectional Valence populations. Like in reward settings, the NAcc FSI threat function remains enigmatic.

By contrast, more consistent firing patterns were observed in putative MSNs. Wide-waveform NAcc neurons more universally suppressed firing during danger cue presentation. Two distinct signals emerged, with Threat Inhibited neurons showing equivalent firing inhibition to danger and uncertainty, but Bidirectional Valence neurons showing preferential firing inhibition to danger. Might these functional types correspond to different neuron types? NAcc MSNs are primarily composed of two genetic types, GABA neurons expressing D_1 versus D_2 receptors. It is tempting to speculate that Bidirectional Valence neurons are D_1-MSNs. Rewarding stimuli are proposed to activate D_1-MSNs to a greater extent than D_2-MSNs (Hikida et al., 2016). NAcc D_1 projections to the ventral pallidum drive cocaine seeking (Pardo-Garcia et al., 2019). Rats will optogenetically self-stimulate NAcc D_1-MSNs at greater rates than D_2-MSNs (Cole et al., 2018). However, the NAcc does not respect the traditional D_1-direct versus D_2-direct pathway like other subregions of the striatum (Kupchik et al., 2015). Both NAcc D_1- and D_2-MSNs project to the ventral pallidum. Depending on the stimulation pattern, D_1- and D_2-MSNs can both drive approach and avoidance behaviors (Soares-Cunha et al., 2020). Even more, a small population of nucleus accumbens neurons appear to express both D_1 and D_2 receptors (Le Moine and Bloch, 1996; Lee et al., 2006). While tempting to speculate Bidirectional Valence neuron identity, any conclusion reached would be premature.

Getting threat information to the NAcc seems obvious, as it receives direct input from the basolateral amygdala (Christie et al., 1987; Kita and Kitai, 1990; Brog et al., 1993; Li et al., 2018). Less obvious is how NAcc threat information is output to a larger network, as there are no reciprocal projections from the NAcc to any amygdala subregion (Basar et al., 2010; Salgado and Kaplitt,

2015). Recent work from our laboratory suggests that the ventral pallidum, which receives direct NAcc inputs, is a compelling candidate (Moaddab et al., 2021). Recording ventral pallidum single-unit activity in the same fear discrimination procedure, we revealed a large functional population signaling relative threat. That is, many ventral pallidum neurons linearly decreased cue firing according to footshock probability. The ventral pallidum is anatomically linked to the amygdala, receiving inputs from the central amygdala (Bourgeais et al., 2001; Knowland et al., 2017; Tooley et al., 2018; Stephenson-Jones et al., 2020) and projecting directly to the basolateral amygdala (Mitrovic and Napier, 1998; Root et al., 2015). The NAcc is necessary to acquire overall fear discrimination, but plays a more selective role in fear expression (Ray et al., 2020). NAcc Threat Inhibited neurons may train up relative threat signaling in the ventral pallidum during acquisition of fear discrimination. An enduring role for NAcc Threat Inhibited neurons may be to rapidly classify safe versus threatening stimuli, reminiscent of rapid NAcc reward processing (Richard et al., 2016; Ottenheimer et al., 2018).

Of course, the ventral pallidum is unlikely the sole recipient of NAcc threat information. The NAcc projects directly to the ventrolateral periaqueductal gray—a region long implicated in fear output—that we are finding to more flexibly signal threat probability (Usuda et al., 1998; Wright et al., 2019; Wright and McDannald, 2019). The NAcc also projects directly to the retrorubral field, a midbrain region housing A8 dopamine neurons (Deutch et al., 1988) that contains diverse signals for threat and aversive outcome (Moaddab and McDannald, 2021). These projections provide a means by which NAcc threat firing may shape firing across a larger threat network and ultimately shape threat behavior.

We set out to reveal NAcc threat firing. At the same time, we were able to record activity around reward delivery, a more familiar setting for investigation of NAcc function. Surprising to us, Bidirectional Valence neurons, showing opposing firing changes to positive and negative valence events, were the most common type. Here we are referring to the valence of predictive cues, rather than outcomes. The footshock cue is obvious—shock was explicitly signaled through sound presentation via speaker. However, reward firing also refers to a predictive auditory cue: the sound of the feeder advance. Thus, both threat and reward firing reflect auditory stimuli preceding biologically significant events. NAcc Bidirectional Valence signaling is reminiscent of dedicated valence signals in the basolateral amygdala, though in the basolateral amygdala, positive and negative valence signals are typically observed in distinct populations (Schoenbaum et al., 1999; Paton et al., 2006; Beyeler et al., 2016; Kim et al., 2016). This includes basolateral amygdala neurons that show similar firing to reward and safety (Sangha et al., 2013). The NAcc may be a site in which parallel inputs for positive and negative valence from the basolateral amygdala converge. Interesting to us, the ventral pallidum also contains Bidirectional Valence neurons (Kaplan et al., 2020; Stephenson-Jones et al., 2020; Moaddab et al., 2021). However, ventral pallidum neurons show more graded firing changes that reflect the degree of threat and reward. The NAcc and ventral pallidum may work in concert, with NAcc neurons bidirectionally classifying valence extremes, and ventral pallidum neurons reporting a Bidirectional Valence gradient spanning threat and reward.

How do we reconcile the existence of Bidirectional Valence neurons with prior work showing separate NAcc valence populations (Setlow et al., 2003) or even overlapping positive and negative valence populations (Roitman et al., 2005)? Recording in an odor discrimination task, Setlow et al. (2003) found that most NAcc neurons acquired firing to an odor predicting quinine (negative valence). NAcc neurons rapidly acquiring selective quinine odor firing had higher baseline firing rates (Setlow et al., 2003). These quinine–cue excited neurons may be FSIs, like our Danger Excited neurons. Negative valence signals generated within the NAcc may span aversive taste and threat.

Recording in a purely pavlovian taste procedure, Roitman et al. (2005) found that most NAcc neurons increased firing to sucrose- and quinine-predictive cues. Even more, most neurons that increased firing to the sucrose-predictive cue also increased firing to the quinine-predictive cue, and vice versa (Roitman et al., 2005). Our Bidirectional Valence findings run completely counter to the findings of Roitman et al. (2005). What may be going on? Although quinine and sucrose cues represent valence extremes, both ultimately control orofacial behavior. A sucrose cue elicits tongue protrusions, mouth movements, swallowing, and additional specific behaviors (Grill and Norgren, 1978; Kerfoot et al., 2007). A quinine cue elicits gaping, rejection movements, and additional behaviors nonoverlapping with the sucrose cue. Bidirectional Valence neurons may increase firing following reward in part to organize specific orofacial and behavioral responding; but a decrease in firing following the danger cue to suppress all forms of taste-related behavior.

Here we have shown that the NAcc contains distinct neuronal populations signaling threat and Bidirectional Valence. Combined with our previous work showing that NAcc activity is necessary for normal fear discrimination (Ray et al., 2020), the present results reveal the NAcc to be an essential component of the threat network of the brain. Our results provide a functional framework for threat and valence processing within the NAcc, working to more fully map neural circuits for threat.

References

Ambroggi F, Ghazizadeh A, Nicola SM, Fields HL (2011) Roles of nucleus accumbens core and shell in incentive-cue responding and behavioral inhibition. J Neurosci 31:6820–6830.

Badrinarayan A, Wescott SA, Vander Weele CM, Saunders BT, Couturier BE, Maren S, Aragona BJ (2012) Aversive stimuli differentially modulate real-time dopamine transmission dynamics within the nucleus accumbens core and shell. J Neurosci 32:15779–15790.

Baldo BA, Kelley AE (2007) Discrete neurochemical coding of distinguishable motivational processes: insights from nucleus accumbens control of feeding. Psychopharmacology (Berl) 191:439–459.

Basar K, Sesia T, Groenewegen H, Steinbusch HWM, Visser-Vandewalle V, Temel Y (2010) Nucleus accumbens and impulsivity. Prog Neurobiol 92:533–557.

Beck CH, Fibiger HC (1995) Conditioned fear-induced changes in behavior and in the expression of the immediate early gene c-fos: with and without diazepam pretreatment. J Neurosci 15:709–720.

Berke JD, Okatan M, Skurski J, Eichenbaum HB (2004) Oscillatory entrainment of striatal neurons in freely moving rats. Neuron 43:883–896.

Berke JD (2008) Uncoordinated firing rate changes of striatal fast-spiking interneurons during behavioral task performance. J Neurosci 28:10075–10080.

Berke JD (2011) Functional properties of striatal fast-spiking interneurons. Front Syst Neurosci 5:45.

Berridge KC (2019) Affective valence in the brain: modules or modes? Nat Rev Neurosci 20:225–234.

Beyeler A, Namburi P, Glober GF, Simonnet C, Calhoon GG, Conyers GF, Luck R, Wildes CP, Tye KM (2016) Divergent routing of positive and negative information from the amygdala during memory retrieval. Neuron 90:348–361.

Blaiss CA, Janak PH (2009) The nucleus accumbens core and shell are critical for the expression, but not the consolidation, of Pavlovian conditioned approach. Behav Brain Res 200:22–32.

Bolles RC (1970) Species-specific defense reactions and avoidance learning. Psychol Rev 77:32–48.
Bolles RC, Collier AC (1976) The effect of predictive cues on freezing in rats. Anim Learn Behav 4:6–8.
Bouchet CA, Miner MA, Loetz EC, Rosberg AJ, Hake HS, Farmer CE, Ostrovskyy M, Gray N, Greenwood BN (2018) Activation of nigrostriatal dopamine neurons during fear extinction prevents the renewal of fear. Neuropsychopharmacology 43:665–672.
Bourgeais L, Gauriau C, Bernard J-F (2001) Projections from the nociceptive area of the central nucleus of the amygdala to the forebrain: a PHA-L study in the rat. Eur J Neurosci 14:229–255.
Bouton ME, Bolles RC (1980) Conditioned fear assessed by freezing and by the suppression of three different baselines. Anim Learn Behav 8:429–434.
Brog JS, Salyapongse A, Deutch AY, Zahm DS (1993) The patterns of afferent innervation of the core and shell in the "accumbens" part of the rat ventral striatum: immunohistochemical detection of retrogradely transported fluoro-gold. J Comp Neurol 338:255–278.
Budygin EA, Park J, Bass CE, Grinevich VP, Bonin KD, Wightman RM (2012) Aversive stimulus differentially triggers subsecond dopamine release in reward regions. Neuroscience 201:331–337.
Cai LX, Pizano K, Gundersen GW, Hayes CL, Fleming WT, Holt S, Cox JM, Witten IB (2020) Distinct signals in medial and lateral VTA dopamine neurons modulate fear extinction at different times. Elife 9:e54936.
Campeau S, Davis M (1995) Involvement of the central nucleus and basolateral complex of the amygdala in fear conditioning measured with fear-potentiated startle in rats trained concurrently with auditory and visual conditioned stimuli. J Neurosci 15:2301–2311.
Carlezon WA, Thomas MJ (2009) Biological substrates of reward and aversion: a nucleus accumbens activity hypothesis. Neuropharmacology 56:122–132.
Cerri DH, Saddoris MP, Carelli RM (2014) Nucleus accumbens core neurons encode value-independent associations necessary for sensory preconditioning. Behav Neurosci 128:567–578.
Chaudhri N, Sahuque LL, Schairer WW, Janak PH (2010) Separable roles of the nucleus accumbens core and shell in context- and cue-induced alcohol-seeking. Neuropsychopharmacology 35:783–791.
Christie MJ, Summers RJ, Stephenson JA, Cook CJ, Beart PM (1987) Excitatory amino acid projections to the nucleus accumbens septi in the rat: a retrograde transport study utilizingd[3H]aspartate and [3H]GABA. Neuroscience 22:425–439.
Cole SL, Robinson MJF, Berridge KC (2018) Optogenetic self-stimulation in the nucleus accumbens: D1 reward versus D2 ambivalence. PLoS One 13: e0207694.
Corbit LH, Balleine BW (2011) The general and outcome-specific forms of pavlovian-instrumental transfer are differentially mediated by the nucleus accumbens core and shell. J Neurosci 31:11786–11794.
Deutch AY, Goldstein M, Baldino F Jr, Roth RH (1988) Telencephalic projections of the A8 dopamine cell group. Ann N Y Acad Sci 537:27–50.
Di Ciano P, Robbins TW, Everitt BJ (2008) Differential effects of nucleus accumbens core, shell, or dorsal striatal inactivations on the persistence, reacquisition, or reinstatement of responding for a drug-paired conditioned reinforcer. Neuropsychopharmacology 33:1413–1425.
Estes KW, Skinner BF (1941) Some quantitative properties of anxiety. J Exp Psychol 29:390–400.
Floresco SB, McLaughlin RJ, Haluk DM (2008) Opposing roles for the nucleus accumbens core and shell in cue-induced reinstatement of food-seeking behavior. Neuroscience 154:877–884.
Fraser KM, Janak PH (2017) Long-lasting contribution of dopamine in the nucleus accumbens core, but not dorsal lateral striatum, to sign-tracking. Eur J Neurosci 46:2047–2055.
Gage GJ, Stoetzner CR, Wiltschko AB, Berke JD (2010) Selective activation of striatal fast-spiking interneurons during choice execution. Neuron 67:466–479.
Gittis AH, Leventhal DK, Fensterheim BA, Pettibone JR, Berke JD, Kreitzer AC (2011) Selective inhibition of striatal fast-spiking interneurons causes dyskinesias. J Neurosci 31:15727–15731.
Gold BP, Mas-Herrero E, Zeighami Y, Benovoy M, Dagher A, Zatorre RJ (2019) Musical reward prediction errors engage the nucleus accumbens and motivate learning. Proc Natl Acad Sci U S A 116:3310–3315.
Grill HJ, Norgren R (1978) The taste reactivity test. I. Mimetic responses to gustatory stimuli in neurologically normal rats. Brain Res 143:263–279.
Groessl F, Munsch T, Meis S, Griessner J, Kaczanowska J, Pliota P, Kargl D, Badurek S, Kraitsy K, Rassoulpour A, Zuber J, Lessmann V, Haubensak W (2018) Dorsal tegmental dopamine neurons gate associative learning of fear. Nat Neurosci 21:952–962.
Hikida T, Morita M, Macpherson T (2016) Neural mechanisms of the nucleus accumbens circuit in reward and aversive learning. Neurosci Res 108:1–5.
Iordanova MD, Westbrook RF, Killcross AS (2006) Dopamine activity in the nucleus accumbens modulates blocking in fear conditioning. Eur J Neurosci 24:3265–3270.
Janak PH, Chen M-T, Caulder T (2004) Dynamics of neural coding in the accumbens during extinction and reinstatement of rewarded behavior. Behav Brain Res 154:125–135.
Kamin LJ, Brimer CJ, Black AH (1963) Conditioned suppression as a monitor of fear of the CS in the course of avoidance training. J Comp Physiol Psychol 56:497–501.
Kaplan A, Mizrahi-Kliger AD, Israel Z, Adler A, Bergman H (2020) Dissociable roles of ventral pallidum neurons in the basal ganglia reinforcement learning network. Nat Neurosci 23:556–564.
Kerfoot EC, Agarwal I, Lee HJ, Holland PC (2007) Control of appetitive and aversive taste-reactivity responses by an auditory conditioned stimulus in a devaluation task: a FOS and behavioral analysis. Learn Mem 14:581–589.
Killcross S, Robbins TW, Everitt BJ (1997) Different types of fear-conditioned behaviour mediated by separate nuclei within amygdala. Nature 388:377–380.
Kim J, Pignatelli M, Xu S, Itohara S, Tonegawa S (2016) Antagonistic negative and positive neurons of the basolateral amygdala. Nat Neurosci 19:1636–1646.
Kita H, Kitai ST (1990) Amygdaloid projections to the frontal-cortex and the striatum in the rat. J Comp Neurol 298:40–49.
Klawonn AM, Malenka RC (2018) Nucleus accumbens modulation in reward and aversion. Cold Spring Harb Symp Quant Biol 83:119–129.
Knowland D, Lilascharoen V, Pacia CP, Shin S, Wang EH-J, Lim BK (2017) Distinct ventral pallidal neural populations mediate separate symptoms of depression. Cell 170:284–297.e18.
Koo JW, Han JS, Kim JJ (2004) Selective neurotoxic lesions of basolateral and central nuclei of the amygdala produce differential effects on fear conditioning. J Neurosci 24:7654–7662.
Krause M, German PW, Taha SA, Fields HL (2010) A pause in nucleus accumbens neuron firing is required to initiate and maintain feeding. J Neurosci 30:4746–4756.
Kriegeskorte N, Mur M, Bandettini PA (2008) Representational similarity analysis—connecting the branches of systems neuroscience. Front Syst Neurosci 2:4.
Kupchik YM, Brown RM, Heinsbroek JA, Lobo MK, Schwartz DJ, Kalivas PW (2015) Coding the direct/indirect pathways by D1 and D2 receptors is not valid for accumbens projections. Nat Neurosci 18:1230–1232.
Lansink CS, Goltstein PM, Lankelma JV, Pennartz CMA (2010) Fast-spiking interneurons of the rat ventral striatum: temporal coordination of activity with principal cells and responsiveness to reward. Eur J Neurosci 32:494–508.
LeDoux JE, Cicchetti P, Xagoraris A, Romanski LM (1990) The lateral amygdaloid nucleus: sensory interface of the amygdala in fear conditioning. J Neurosci 10:1062–1069.
Le Moine C, Bloch B (1996) Expression of the D3 dopamine receptor in peptidergic neurons of the nucleus accumbens: comparison with the D1 and D2 dopamine receptors. Neuroscience 73:131–143.
Lee K-W, Kim Y, Kim AM, Helmin K, Nairn AC, Greengard P (2006) Cocaine-induced dendritic spine formation in D1 and D2 dopamine receptor-containing medium spiny neurons in nucleus accumbens. Proc Natl Acad Sci U S A 103:3399–3404.
Levita L, Dalley JW, Robbins TW (2002) Disruption of Pavlovian contextual conditioning by excitotoxic lesions of the nucleus accumbens core. Behav Neurosci 116:539–552.
Li Z, Chen Z, Fan G, Li A, Yuan J, Xu T (2018) Cell-type-specific afferent innervation of the nucleus accumbens core and shell. Front Neuroanat 12:84.
Lobo MK, Covington HE III, Chaudhury D, Friedman AK, Sun H, Damez-Werno D, Dietz DM, Zaman S, Koo JW, Kennedy PJ, Mouzon E, Mogri M, Neve RL, Deisseroth K, Han M-H, Nestler EJ (2010) Cell type–specific

loss of BDNF signaling mimics optogenetic control of cocaine reward. Science 330:385–390.
Mannella F, Gurney K, Baldassarre G (2013) The nucleus accumbens as a nexus between values and goals in goal-directed behavior: a review and a new hypothesis. Front Behav Neurosci 7:135.
Martinez RCR, Oliveira AR, Macedo CE, Molina VA, Brandão ML (2008) Involvement of dopaminergic mechanisms in the nucleus accumbens core and shell subregions in the expression of fear conditioning. Neurosci Lett 446:112–116.
McAllister KH (1997) A single administration of d-amphetamine prior to stimulus pre-exposure and conditioning attenuates latent inhibition. Psychopharmacology (Berl) 130:79–84.
McGinty VB, Lardeux S, Taha SA, Kim JJ, Nicola SM (2013) Invigoration of reward seeking by cue and proximity encoding in the nucleus accumbens. Neuron 78:910–922.
Mitrovic I, Napier TC (1998) Substance P attenuates and DAMGO potentiates amygdala glutamatergic neurotransmission within the ventral pallidum. Brain Res 792:193–206.
Moaddab M, McDannald MA (2021) Retrorubral field is a hub for diverse threat and aversive outcome signals. Curr Biol 31:2099–2110.e5.
Moaddab M, Hyland BI, Brown CH (2015) Oxytocin excites nucleus accumbens shell neurons in vivo. Mol Cell Neurosci 68:323–330.
Moaddab M, Ray MH, McDannald MA (2021) Ventral pallidum neurons dynamically signal relative threat. Commun Biol 4:43.
Morrow K, Dinavahi M, Kim J, Song S, Hu K, Pessoa L (2021) Distributed and multifaceted effects of threat and safety. bioRxiv. Advance online publication. Retrieved November 10, 2021. .
Nicola SM, Yun IA, Wakabayashi KT, Fields HL (2004) Cue-evoked firing of nucleus accumbens neurons encodes motivational significance during a discriminative stimulus task. J Neurophysiol 91:1840–1865.
Ottenheimer D, Richard JM, Janak PH (2018) Ventral pallidum encodes relative reward value earlier and more robustly than nucleus accumbens. Nat Commun 9:4350.
Pardo-Garcia TR, Garcia-Keller C, Penaloza T, Richie CT, Pickel J, Hope BT, Harvey BK, Kalivas PW, Heinsbroek JA (2019) Ventral pallidum is the primary target for accumbens D_1 projections driving cocaine seeking. J Neurosci 39:2041–2051.
Parkinson JA, Olmstead MC, Burns LH, Robbins TW, Everitt BJ (1999a) Dissociation in effects of lesions of the nucleus accumbens core and shell on appetitive pavlovian approach behavior and the potentiation of conditioned reinforcement and locomotor activity by D-amphetamine. J Neurosci 19:2401–2411.
Parkinson JA, Robbins TW, Everitt BJ (1999b) Selective excitotoxic lesions of the nucleus accumbens core and shell differentially affect aversive Pavlovian conditioning to discrete and contextual cues. Psychobiology 27:256–266.
Parkinson JA, Willoughby PJ, Robbins TW, Everitt BJ (2000) Disconnection of the anterior cingulate cortex and nucleus accumbens core impairs Pavlovian approach behavior: further evidence for limbic cortical-ventral striatopallidal systems. Behav Neurosci 114:42–63.
Paton JJ, Belova MA, Morrison SE, Salzman CD (2006) The primate amygdala represents the positive and negative value of visual stimuli during learning. Nature 439:865–870.
Pauli WM, Larsen T, Collette S, Tyszka JM, Seymour B, O'Doherty JP (2015) Distinct contributions of ventromedial and dorsolateral subregions of the human substantia nigra to appetitive and aversive learning. J Neurosci 35:14220–14233.
Paxinos G, Watson C (2007) The rat brain in stereotaxic coordinates, Ed 6. Amsterdam: Academic/Elsevier.
Piantadosi PT, Yeates DCM, Floresco SB (2020) Prefrontal cortical and nucleus accumbens contributions to discriminative conditioned suppression of reward-seeking. Learn Mem 27:429–440.
Ray MH, Russ AN, Walker RA, McDannald MA (2020) The nucleus accumbens core is necessary to scale fear to degree of threat. J Neurosci 40:4750–4760.
Reynolds SM, Berridge KC (2002) Positive and negative motivation in nucleus accumbens shell: bivalent rostrocaudal gradients for GABA-elicited eating, taste "liking"/"disliking" reactions, place preference/avoidance, and fear. J Neurosci 22:7308–7320.
Richard JM, Ambroggi F, Janak PH, Fields HL (2016) Ventral pallidum neurons encode incentive value and promote cue-elicited instrumental actions. Neuron 90:1165–1173.
Ritchey M, Wing EA, LaBar KS, Cabeza R (2013) Neural similarity between encoding and retrieval is related to memory via hippocampal interactions. Cereb Cortex 23:2818–2828.
Roesch MR, Singh T, Brown PL, Mullins SE, Schoenbaum G (2009) Ventral striatal neurons encode the value of the chosen action in rats deciding between differently delayed or sized rewards. J Neurosci 29:13365–13376.
Roitman MF, Wheeler RA, Carelli RM (2005) Nucleus accumbens neurons are innately tuned for rewarding and aversive taste stimuli, encode their predictors, and are linked to motor output. Neuron 45:587–597.
Root DH, Melendez RI, Zaborszky L, Napier TC (2015) The ventral pallidum: subregion-specific functional anatomy and roles in motivated behaviors. Prog Neurobiol 130:29–70.
Saeb-Parsy K, Dyball REJ (2003) Defined cell groups in the rat suprachiasmatic nucleus have different day/night rhythms of single-unit activity in vivo. J Biol Rhythms 18:26–42.
Salgado S, Kaplitt MG (2015) The nucleus accumbens: a comprehensive review. Stereotact Funct Neurosurg 93:75–93.
Sangha S, Chadick JZ, Janak PH (2013) Safety encoding in the basal amygdala. J Neurosci 33:3744–3751.
Schoenbaum G, Setlow B (2003) Lesions of nucleus accumbens disrupt learning about aversive outcomes. J Neurosci 23:9833–9841.
Schoenbaum G, Chiba AA, Gallagher M (1999) Neural encoding in orbitofrontal cortex and basolateral amygdala during olfactory discrimination learning. J Neurosci 19:1876–1884.
Schwienbacher I, Fendt M, Richardson R, Schnitzler HU (2004) Temporary inactivation of the nucleus accumbens disrupts acquisition and expression of fear-potentiated startle in rats. Brain Res 1027:87–93.
Setlow B, Schoenbaum G, Gallagher M (2003) Neural encoding in ventral striatum during olfactory discrimination learning. Neuron 38:625–636.
Sicre M, Meffre J, Louber D, Ambroggi F (2020) The nucleus accumbens core is necessary for responding to incentive but not instructive stimuli. J Neurosci 40:1332–1343.
Soares-Cunha C, de Vasconcelos NAP, Coimbra B, Domingues AV, Silva JM, Loureiro-Campos E, Gaspar R, Sotiropoulos I, Sousa N, Rodrigues AJ (2020) Nucleus accumbens medium spiny neurons subtypes signal both reward and aversion. Mol Psychiatry 25:3241–3255.
Sosa M, Joo HR, Frank LM (2020) Dorsal and ventral hippocampal sharp-wave ripples activate distinct nucleus accumbens networks. Neuron 105:725–741.e8.
Stephenson-Jones M, Bravo-Rivera C, Ahrens S, Furlan A, Xiao X, Fernandes-Henriques C, Li B (2020) Opposing contributions of GABAergic and glutamatergic ventral pallidal neurons to motivational behaviors. Neuron 105:921–933.e5.
Strong CE, Hagarty DP, Brea Guerrero A, Schoepfer KJ, Cajuste SM, Kabbaj M (2020) Chemogenetic selective manipulation of nucleus accumbens medium spiny neurons bidirectionally controls alcohol intake in male and female rats. Sci Rep 10:19178.
Sugam JA, Saddoris MP, Carelli RM (2014) Nucleus accumbens neurons track behavioral preferences and reward outcomes during risky decision making. Biol Psychiatry 75:807–816.
Taha SA, Fields HL (2005) Encoding of palatability and appetitive behaviors by distinct neuronal populations in the nucleus accumbens. J Neurosci 25:1193–1202.
Thomas KL, Hall J, Everitt BJ (2002) Cellular imaging with zif268 expression in the rat nucleus accumbens and frontal cortex further dissociates the neural pathways activated following the retrieval of contextual and cued fear memory. Eur J Neurosci 16:1789–1796.
Tooley J, Marconi L, Alipio JB, Matikainen-Ankney B, Georgiou P, Kravitz AV, Creed MC (2018) Glutamatergic ventral pallidal neurons modulate activity of the habenula–tegmental circuitry and constrain reward seeking. Biol Psychiatry 83:1012–1023.
Usuda I, Tanaka K, Chiba T (1998) Efferent projections of the nucleus accumbens in the rat with special reference to subdivision of the nucleus: biotinylated dextran amine study. Brain Res 797:73–93.
Vachez YM, Tooley JR, Abiraman K, Matikainen-Ankney B, Casey E, Earnest T, Ramos LM, Silberberg H, Godynyuk E, Uddin O, Marconi L, Le Pichon CE, Creed MC (2021) Ventral arkypallidal neurons inhibit accumbal firing to promote reward consumption. Nat Neurosci 24:379–390.
Vento PJ, Jhou TC (2020) Bidirectional valence encoding in the ventral pallidum. Neuron 105:766–768.

Vetere G, Kenney JW, Tran LM, Xia F, Steadman PE, Parkinson J, Josselyn SA, Frankland PW (2017) Chemogenetic interrogation of a brain-wide fear memory network in mice. Neuron 94:363–374.e4.

Voorn P, Gerfen CR, Groenewegen HJ (1989) Compartmental organization of the ventral striatum of the rat: immunohistochemical distribution of enkephalin, substance P, dopamine, and calcium-binding protein. J Comp Neurol 289:189–201.

Walker RA, Andreansky C, Ray MH, McDannald MA (2018) Early adolescent adversity inflates threat estimation in females and promotes alcohol use initiation in both sexes. Behav Neurosci 132:171–182.

Walker RA, Wright KM, Jhou TC, McDannald MA (2019) The ventrolateral periaqueductal gray updates fear via positive prediction error. Eur J Neurosci 51:866–880.

Wendler E, Gaspar JCC, Ferreira TL, Barbiero JK, Andreatini R, Vital MABF, Blaha CD, Winn P, Da Cunha C (2014) The roles of the nucleus accumbens core, dorsomedial striatum, and dorsolateral striatum in learning: performance and extinction of Pavlovian fear-conditioned responses and instrumental avoidance responses. Neurobiol Learn Mem 109:27–36.

Wenzel JM, Rauscher NA, Cheer JF, Oleson EB (2015) A role for phasic dopamine release within the nucleus accumbens in encoding aversion: a review of the neurochemical literature. ACS Chem Neurosci 6:16–26.

Wright KM, McDannald MA (2019) Ventrolateral periaqueductal gray neurons prioritize threat probability over fear output. Elife 8:e45013.

Wright KM, Jhou TC, Pimpinelli D, McDannald MA (2019) Cue-inhibited ventrolateral periaqueductal gray neurons signal fear output and threat probability in male rats. Elife 8:e50054.

Yarom O, Cohen D (2011) Putative cholinergic interneurons in the ventral and dorsal regions of the striatum have distinct roles in a two choice alternative association task. Frontiers in Systems Neuroscience 5:36.

Zahm DS, Brog JS (1992) On the significance of subterritories in the "accumbens" part of the rat ventral striatum. Neuroscience 50:751–767.

Zhang Y, Zhu Y, Cao S-X, Sun P, Yang J-M, Xia Y-F, Xie S-Z, Yu X-D, Fu J-Y, Shen C-J, He H-Y, Pan H-Q, Chen X-J, Wang H, Li X-M (2020) MeCP2 in cholinergic interneurons of nucleus accumbens regulates fear learning. Elife 9:e55342.